

Line-driven radiative outflows in luminous quasars

Rebecca A. A. Bowler^{1,2*}, Paul C. Hewett¹, James T. Allen^{1,3} and Gary J. Ferland^{4,5}

1. Institute of Astronomy, University of Cambridge, Cambridge CB3 0HA

2. SUPA†, Institute for Astronomy, University of Edinburgh, Royal Observatory, Edinburgh EH9 3HJ

3. Sydney Institute for Astronomy, School of Physics, A28, University of Sydney, NSW 2006, Australia

4. Department of Physics and Astronomy, University of Kentucky, Lexington, KY 40506, USA

5. Centre for Theoretical Atomic, Molecular and Optical Physics, School of Mathematics and Physics, Queens University Belfast, Belfast BT7 1NN, UK

6 June 2021

ABSTRACT

An analysis of $\simeq 19\,500$ narrow ($\lesssim 200\text{ km s}^{-1}$) C IV $\lambda\lambda 1548.2, 1550.8$ absorbers in $\simeq 34\,000$ Sloan Digital Sky Survey quasar spectra is presented. The statistics of the number of absorbers as a function of outflow-velocity shows that in approximately two-thirds of outflows, with multiple C IV absorbers present, absorbers are line-locked at the 500 km s^{-1} velocity separation of the C IV absorber doublet; appearing as ‘triplets’ in the quasar spectra. Line-locking is an observational signature of radiative line driving in outflowing material, where the successive shielding of ‘clouds’ of material in the outflow locks the clouds together in outflow velocity. Line-locked absorbers are seen in both broad absorption line quasars (BALs) and non-BAL quasars with comparable frequencies and with velocities out to at least $20\,000\text{ km s}^{-1}$. There are no detectable differences in the absorber properties and the dust content of single C IV doublets and line-locked C IV doublets. The gas associated with both single and line-locked C IV absorption systems includes material with a wide range of ionization potential (14–138 eV). Both single and line-locked C IV absorber systems show strong systematic trends in their ionization as a function of outflow velocity, with ionization decreasing rapidly with increasing outflow velocity. Initial simulations, employing CLOUDY, demonstrate that a rich spectrum of line-locked signals at various velocities may be expected due to significant opacities from resonance lines of Li-, He- and H-like ions of O, C and N, along with contributions from He II and H I resonance lines. The simulations confirm that line driving can be the dominant acceleration mechanism for clouds with $N(\text{H I}) \simeq 10^{19}\text{ cm}^{-2}$.

Key words: galaxies: active - quasars: absorption lines

1 INTRODUCTION

Evidence for highly ionized outflowing material is seen in the rest-frame ultra-violet spectral energy distributions (SEDs) of many quasars. Outflows are most prominent in broad absorption line quasars (BALQSOs), where extensive line absorption by matter at outflow velocities up to $30\,000\text{ km s}^{-1}$ is seen as a broad trough blueward of the rest-frame emission from the quasar (Weymann et al. 1991). BALQSOs themselves are observed to make up some 20 per cent of the population (e.g. Hewett & Foltz 2003) and the intrinsic fraction of BALQSOs is even higher at redshifts $z \gtrsim 3$ (Allen et al. 2011). The ubiquitous presence of outflows with velocities up to $12\,000\text{ km s}^{-1}$, visible via their absorption in the C IV $\lambda\lambda 1548.19, 1550.77$ doublet¹ (Nestor, Hamann & Rodríguez Hidalgo 2008; Wild et al. 2008)

suggests the estimate that 60 per cent of quasars possess outflows in the review by Ganguly & Brotherton (2008) may be conservative.

While the evidence for the presence of outflows associated with the majority of quasars is established, the origin, dynamics and composition of such outflows are poorly constrained. Models based on radiation driven flows (Shlosman, Vitello, & Shaviv 1985; Arav, Li, & Begelman 1994; Murray et al. 1995; Proga, Stone, & Kallman 2000; Chelouche & Netzer 2001), magnetohydrodynamic driven winds (Blandford & Payne 1982; Emmering, Blandford, & Shlosman 1992; Konigl & Kartje 1994; Bottorff et al. 1997) and thermal winds (Proga 2007) all remain viable and it is possible that more than one mechanism is important.

The quantity of material expelled from the central region of the quasar, and the energy it carries, has important implications for determining the lifetime of the quasar, the composition of the interstellar medium (ISM) and galactic feedback mechanisms. Ostriker et al. (2010) provide a recent review of the key physical quantities involved.

* E-mail: raab@roe.ac.uk

† Scottish Universities Physics Alliance

¹ Vacuum wavelengths are used throughout the paper

Information about the nature of outflows, and the importance of radiative driving in their generation, can be gained from an analysis of the observed velocity structures present in the outflowing material. Radiation-driving, and particularly the importance of acceleration via the interaction of photons with bound electrons in the outflowing material, is perhaps most familiar as the mechanism for producing winds from hot stars. Castor, Abbott, & Klein (1975) presented the theory for stars at a time when spectroscopic observations of quasars were just beginning to provide observational constraints on the properties of gaseous material associated with the objects (Burbidge & Burbidge 1975).

Compared to the situation with hot stars, the geometry of outflows in quasars is likely more complex and there are key differences in the physical properties of the outflowing material, notably the much lower particle densities. The theory behind radiatively-driven winds for quasars was developed by Arav and coworkers in the 1990s (Arav & Li 1994; Arav, Li, & Begelman 1994). The importance of radiation-driving for outflows in BALQSOs was stressed (Arav et al. 1995) and Arav (1996) proposed the detection of the ‘ghost of Ly α ’ as unambiguous evidence for radiation-driving as the dominant source of acceleration in BALQSO winds. The phenomenon is postulated to arise in outflows where absorption of Ly α photons by N V-ions at a velocity of $\simeq 5900 \text{ km s}^{-1}$ (where, in the frame of the outflowing N V-ions, strong resonant absorption occurs) results in the rapid acceleration of material to greater velocities, reducing the amount of material present. The overall absorption opacity at $\simeq 5900 \text{ km s}^{-1}$ is thereby reduced and an excess of emission is visible (e.g. see figure 1 of Arav 1996). For a tracer-ion in the flow, such as C IV, the manifestation of the phenomenon is a reduction in the absorption at $\simeq 5900 \text{ km s}^{-1}$, leading to an apparent local excess of continuum emission; hence the ‘ghost of Ly α ’ name.

The in-depth consideration of the phenomenon by Arav (1996) was motivated in part by possible differences in the spectra of non-BALQSOs and BALQSOs presented by Weymann et al. (1991) and the subsequent investigation of Korista et al. (1993). As discussed by Arav (1996), very specific conditions are necessary for the ‘ghost of Ly α ’ to be detected. An outflow, including significant N V absorption, extending to $\sim 10\,000 \text{ km s}^{-1}$, must be present in a quasar that possesses both strong and relatively narrow intrinsic Ly α emission. The ghost signature is predicted to be most obvious for quasars where the far-ultraviolet spectrum of the quasar is weak, suppressing any contribution to the acceleration of the outflow from additional absorption due to resonance lines with wavelengths $< 1000 \text{ \AA}$.

Observational evidence for the presence of the ghost of Ly α has proved elusive, even when a systematic approach, using the power of the very large sample of homogeneous, moderate resolution and moderate signal-to-noise ratio spectra of quasars (Schneider et al. 2010) from the Sloan Digital Sky Survey (SDSS) are employed (Cottis et al. 2010).

In this paper, we undertake a complementary search, focused on the presence of ‘line-locked’ absorption features in the spectra of individual quasars with extended narrow line absorption. Such line-locked absorption is also accepted as evidence that radiative line-driving plays an important role in quasar outflow dynamics (Benn et al. 2005; Foltz et al. 1987).

The principle behind line-locking in radiatively-driven outflows is that, under certain circumstances, material closer to the origin of the outflow can shield material further out, resulting in a synchronising of the outflow velocities. Specifically, if a distant ‘cloud’ is being accelerated outwards by line-

driving arising from resonant absorption of photons in a particular ionic species, the reduction in the flux received by this cloud due to shielding by an inner cloud, moving with a relative velocity equivalent to the separation of two prominent absorption lines, could cause the clouds to become locked together in velocity (Milne 1926; Scargle 1973; Braun & Milgrom 1989). Simulations of the structure, dynamics and origin of quasar outflows also indicate that, for radiatively driven flows, line-locking could be prevalent (Chelouche & Netzer 2003). Quasar outflows are almost certainly quite complex and simulations (e.g. Proga, Ostriker, & Kurosawa 2008; Kurosawa & Proga 2009; Proga et al. 2014) predict the presence of significant structure on a variety of scales, involving fragmentation and clumping, some of which may be highly non-spherical (e.g. filamentary or pancake-like). Our use of the ‘cloud’-terminology above, and later in the paper, is as a shorthand for some form of modulation in density within the flow, along the line-of-sight to the illuminating source.

The potential significance of observing a clear signature of line-locking has been recognised (Burbidge & Burbidge 1975) for much of the period since the discovery of quasars. Evidence for the presence of line-locking signatures have, however, been largely confined to the identification of ‘picket fence’-type absorption configurations in a relatively small number of individual quasars (e.g. Williams et al. 1975; Coleman et al. 1976; Adams et al. 1978; Foltz et al. 1987; Borra et al. 1996; Tripp, Lu, & Savage 1997; Srikanand 2000; Fechner, Baade, & Reimers 2004; Benn et al. 2005; Simon & Hamann 2010; Hamann et al. 2011).

The availability of the SDSS spectroscopic quasar sample (Schneider et al. 2010) now allows quantitative statistical investigation of outflow absorption signatures to be undertaken. We focus on the properties of absorption due to triply-ionized carbon, specifically the doublet transition C IV $\lambda\lambda 1548.19, 1550.77$, which is the most readily observable high-ionization absorption feature in the SDSS spectra that appears longward of the effects of the Ly α -forest (below $\simeq 1200 \text{ \AA}$).

The nature of C IV absorption in BALQSOs and non-BALQSOs is dramatically different and we analyse samples of BALQSOs and non-BALQSOs separately. Initially we began the investigation using an auto-correlation calculation, designed to be sensitive to the presence of many, individually difficult to detect, faint absorption features. More specifically, we looked for correlations between ‘absorber pixels’ as a function of velocity separation, within each quasar spectrum, without the need to pre-identify individual, discrete absorbers. The auto-correlation method was devised primarily for BALQSOs, which represent a subset of the quasar population where outflows of material are very definitely present, yet the complex absorption profiles of the BAL-troughs mean that searches for discrete absorbers might not represent the optimum approach. In practice, such a reservation turned out to be unfounded and, as a result, we employed the familiar approach of identifying discrete absorption features and then investigating the incidence of absorber ‘pairs’ as a function of velocity separation. The discrete-absorber method turns out to be highly effective for the investigation of the properties of individual, relatively narrow, C IV-absorbers present in both the non-BALQSO and BALQSO quasar samples.

The paper is structured as follows. First, we present the SDSS quasar sample in Section 2. The absorption line identification scheme is described in Section 3. Statistics of the population of C IV-absorbers as a function of outflow velocity are presented in Section 4. In Section 5, we create and analyse composite quasar spectra as a function of outflow velocity, allowing an investigation

into the physical properties of the absorbers and the host quasars. Line-locking is shown to be almost ubiquitous among narrow C IV absorbers in quasar outflows with multiple absorbers. A discussion of the interpretation of the results, including exploratory simulations using CLOUDY, is presented in Section 6, before the main conclusions of the paper are summarised in Section 7.

2 THE QUASAR SAMPLE

The base quasar sample consisted of 42 273 objects with redshifts $1.54 \leq z \leq 3.0$ from the DR7 quasar catalogue of Schneider et al. (2010), where the lower redshift limit was imposed in order for the blue-wing of the C IV emission line to lie within the SDSS spectra. Above redshift $z = 3.0$ the number of quasars in the SDSS catalogue drops rapidly, and the majority are fainter than their lower redshift counterparts resulting in a significant reduction in the signal-to-noise ratio (S/N) of the spectra. The quasars possess absolute magnitudes in the range $-23.0 \leq M_i \leq -29.5$ (Shen et al. 2011) but the sample is predominantly (79 per cent) made up of objects with $-25.0 \leq M_i \leq -27.0$.

The spectra were all processed through the sky-residual subtraction scheme of Wild & Hewett (2005), which results in significantly improved S/N at observed wavelengths $\lambda > 7200 \text{ \AA}$, contributing to the estimation of more accurate quasar redshifts² from Hewett & Wild (2010), which are employed throughout. For 3581 quasars in the sample, the SDSS DR7 release includes multiple spectra of high quality. For these quasars, the spectra were co-added using inverse variance weighting to produce a combined spectrum with improved S/N. All spectra were also corrected for the effects of Galactic extinction using the SDSS $E(B-V)$ measurement, taken from the dust maps of Schlegel, Finkbeiner, & Davis (1998), and the Milky Way extinction curve of Cardelli, Clayton & Mathis (1989).

The sample was culled to remove objects with spectra of low S/N in which the majority of moderate equivalent width C IV absorption features are not readily detectable. Specifically, spectra were retained in the sample if the average S/N per pixel in the continuum redward of the C IV emission, at 1600-1650 \AA , exceeded $S/N=5.0$. To eliminate objects possessing spectra with extended wavelength regions missing, spectra with fewer than 3500 pixels (defined by the SDSS-flag *NGOOD*) were also excluded. Application of the two criterion resulted in the removal of 8477 spectra, leaving a sample of 33 796 quasars.

Samples of non-BALQSOs and BALQSOs were defined using the classifications of Allen et al. (2011) for quasars present in the SDSS DR6 release. The small fraction of quasars present only in DR7 were classified via visual inspection³. The resulting subsamples of non-BALQSOs and BALQSOs contained 31 142 and 2654 quasars respectively.

The SDSS spectra are supplied on a logarithmic wavelength scale, with pixels of 69 km s^{-1} width. When defining reference wavelengths, or generating composite spectra in the quasar rest-frame, nearest-pixel values were employed and no interpolation or rebinning was performed at any stage.

3 THE ABSORBER SAMPLE

3.1 Absorption line detection

Discrete absorption features were identified using the following scheme. A ‘continuum’ is defined for each quasar via the application of a simple 41-pixel median filter. The ‘difference’ spectrum, to be searched for absorption features, is then obtained by subtracting the continuum from the original quasar spectrum. The absorption line search uses a matched-filter technique (e.g. Hewett et al. 1985) with template Gaussian profiles of full width at half maximum (FWHM) = 160 km s^{-1} (the resolution of the SDSS spectra), 200 km s^{-1} and 240 km s^{-1} . Templates with lines centred at half-pixel (i.e. 34.5 km s^{-1}) intervals are employed, allowing the absorber centroids to be located to better than $\pm 34.5 \text{ km s}^{-1}$. At each half-pixel, the template giving the minimum χ^2 value is determined and candidate absorbers are selected by applying a detection-threshold of $S/N \geq 3$, where the noise is calculated using the array of variance values included with each SDSS spectrum. The low value of the S/N-threshold is chosen deliberately to ensure the inclusion of as many real features as possible, albeit at the expense of the presence of a population of spurious ‘detections’.

The combination of the finite resolution of the quasar spectra and the intrinsic velocity widths of absorption systems precludes the detection of pairs of absorbers with small velocity separations. Two unresolved absorbers must be at least $\simeq 5$ -pixels ($\simeq 345 \text{ km s}^{-1}$) apart to be detected as distinct features⁴ and the ‘exclusion’ interval becomes somewhat larger for features that are resolved, i.e. possess intrinsic velocity widths $\gtrsim 100 \text{ km s}^{-1}$. A C IV doublet was defined from the presence of two absorption features separated by 7.24 ± 1.00 pixels. The C IV doublet velocity separation of 500 km s^{-1} (i.e. 7.24 pixels in the SDSS spectra) is such that C IV absorbers with intrinsic velocity widths of up to $\simeq 200 \text{ km s}^{-1}$ are detectable, hence the maximum template velocity width of 240 km s^{-1} used for absorber detection. Real C IV doublets with larger observed velocity widths no longer appear as two separate, individual, absorbers and are thus not included in the doublet catalogue.

The rest-frame equivalent width (EW_{1548})-limit reached depends on the S/N of the individual quasar spectra. The absorber sample is essentially complete for the EW_{1548} -interval $0.4 < EW_{1548} < 1.0 \text{ \AA}$. At lower EW_{1548} , the sample becomes increasingly incomplete; the number of absorbers detected reaches a maximum at $EW_{1548}=0.3 \text{ \AA}$, below which the number of systems detected declines precipitately towards the minimum EW included in the non-BALQSO sample of $EW_{1548}=0.1 \text{ \AA}$. Above $EW_{1548}=1.0 \text{ \AA}$ the sample also rapidly becomes incomplete because of the maximum velocity width (FWHM = 240 km s^{-1}) of the detection templates, imposed to ensure that the components of the C IV doublets remain resolved.

For the BALQSO sample the catalogue of narrow absorbers is less complete because of the presence of significant absorption, of substantial optical depth, over much larger velocity intervals. Less than 1 percent of the C IV doublets were excluded from the non-BALQSO sample by applying the $EW_{1548} \geq 0.1 \text{ \AA}$ condition, and, given the difficulty of defining a meaningful EW-estimate for many of the narrow absorbers lying within broader absorption features,

² http://www.sdss.org/dr7/products/value_added/index.html/#quasars

³ None of the results presented are sensitive to the exact definition of the BALQSO and non-BALQSO samples.

⁴ A more sophisticated, multi-component scheme to identify closer absorbers is in principle possible, but neither the scientific goal or the quality of the spectra merit such an approach.

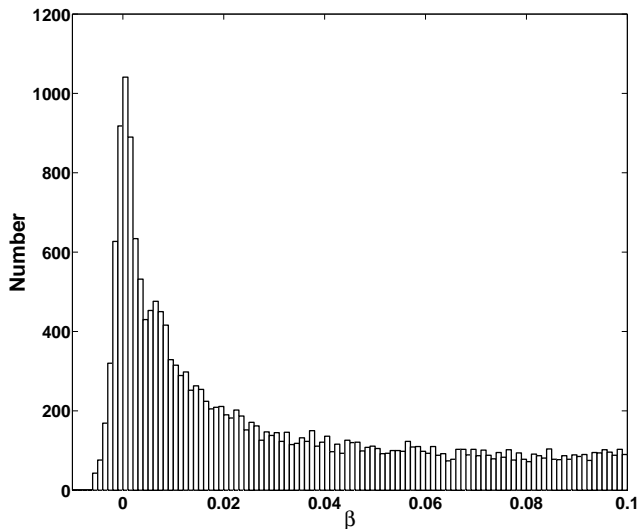


Figure 1. The distribution of the full sample of 18 908 C IV absorbers as a function of outflow velocity, $\beta = v/c$, identified in the sample of 31 142 non-BALQSOs. The majority of C IV absorbers with $\beta > 0.05$ are expected to arise in intervening galaxy haloes, unrelated to the quasars. The excess of apparently outflowing absorbers is present out to at least $\beta = 0.04$. An excess of C IV absorbers with a relatively low velocity-dispersion ($\sigma_{\text{observed}} \simeq 500 \text{ km s}^{-1}$ —including remaining quasar redshift errors) centred on the quasar systemic velocity is also evident from employing the improved quasar redshifts of Hewett & Wild (2010).

no EW_{1548} -limit was applied to the absorber catalogue from the BALQSO sample.

Investigation of the number of line-locked C IV systems within the absorber catalogue is differential in nature and determination of the exact completeness of the C IV absorber sample as a function of EW_{1548} does not affect the results presented. The key factor is that the relative probabilities of detecting C IV doublets and C IV triplets (i.e. potentially line-locked systems) are well determined. None of the results presented in the paper change, other than the exact number of absorbers involved, if the absorber sample is restricted to minimum EW_{1548} thresholds of up to 0.4 \AA . Results from the full sample, to a minimum $\text{EW}_{1548} = 0.1 \text{ \AA}$, are presented to maximise the number of C IV absorbers involved and hence the S/N of the results for both doublet and triplet absorbers.

The absorber sample has properties very similar to other C IV absorber samples derived recently from SDSS spectra (e.g. Cooksey et al. 2013), although the scheme for continuum determination and feature finding are somewhat different. The apparent optical depth method (Savage & Sembach 1991) leads to an estimate of the minimum column densities reached of $\log(N_{\text{CIV}}) \simeq 14.0$.

3.2 Absorber outflow velocities

The outflow/inflow velocity of a C IV absorber, detected at wavelength λ_{abs} in a rest-frame quasar spectrum, is parametrized by $\beta = v/c \simeq (1548.19 - \lambda_{\text{abs}})/1548.19$, where c is the velocity of light and 1548.19 \AA is the rest-frame wavelength of the blue component of the C IV doublet. An outflowing absorber has positive β and the C IV absorber search was undertaken for $\beta \leq 0.1$, i.e. to $v \simeq 30\,000 \text{ km s}^{-1}$. At larger β , the presence of absorption due to Si IV $\lambda\lambda\ 1393.8, 1402.8$ increases the number of spurious C IV absorber detections, particularly in the BALQSO sample. The significantly improved errors in the quasar redshifts (Hewett & Wild

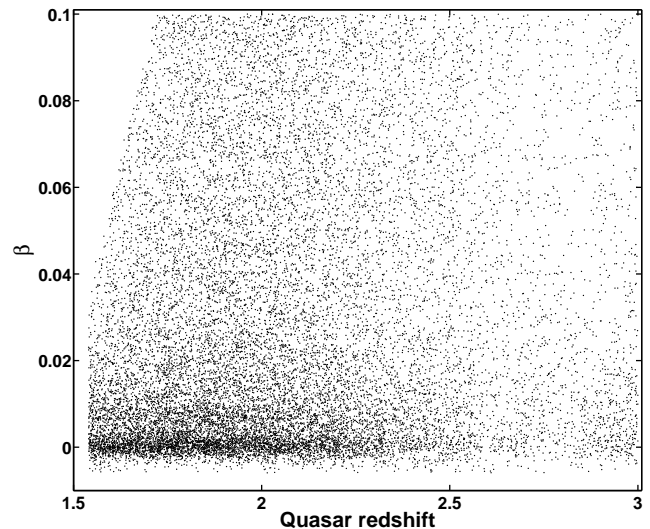


Figure 2. The 18 908 C IV absorbers in the non-BALQSO sample plotted as a function of the quasar redshift and outflow velocity, β . The absence of absorbers at large β for quasar redshifts $z < 1.75$ results from the minimum observed-frame wavelength of $\simeq 3810 \text{ \AA}$ included in the SDSS spectra.

2010) reduces the number of apparently infalling absorbers (with negative β) dramatically. Absorbers are still, however, detected with negative β due to i) remaining quasar redshift errors, ii) the presence of ‘associated’ C IV absorbers that are not participating in an outflow, and iii) [potentially] infalling C IV absorbers. The distribution of 18 908 C IV absorbers in the non-BALQSO sample as a function of β is shown in Fig. 1 and the distribution as a function of the quasar redshift and β is shown in Fig. 2. Throughout the paper, the statistics given for absorbers apply to those with $\beta \geq 0$, unless otherwise stated.

Nestor, Hamann & Rodríguez Hidalgo (2008) drew attention to the shape of the C IV absorber distribution at small β (their figs. 5 and 6). The twin-peak, or, equivalently, reduced number of outflow absorbers at $v < 2000 \text{ km s}^{-1}$ ($\beta < 0.00667$) is confirmed at high significance in Fig. 1. The apparent two-component nature of the absorber velocity distribution is perhaps most evident in Fig. 2, where the much larger number of absorbers and the effect of the improved redshift accuracy for the quasars, confirms the presence of a significant absorber population centred on the systemic quasar redshift and the presence of an apparent maximum in the outflow absorber population at $\simeq 0.00667$. Analysis of the different absorber populations is beyond the scope of the results presented here, but further investigation of C IV absorbers employing the significant statistical power of the new SDSS DR10 quasar sample (Páris et al. 2014) will be forthcoming.

Our absorption line detection routine resulted in samples of 16 762 (2637) C IV doublets ($0.0 \leq \beta \leq 0.1$) from the 31 142 (2654) non-BALQSO (BAL) spectra respectively. In Fig. 3 we show the arithmetic-mean composite absorption-line spectrum of 5098 C IV absorbers with $0.04 < \beta < 0.1$ identified in the non-BALQSO sample. The individual quasars containing the absorbers were normalised using a high-S/N quasar composite (see Section 5 for details) and combined, after shifting the normalised-spectra to the rest-frame of the absorbers. Numerous additional absorption features from other ions associated with the C IV systems, covering a range of ionization potential, are visible in the high-S/N composite spectrum.

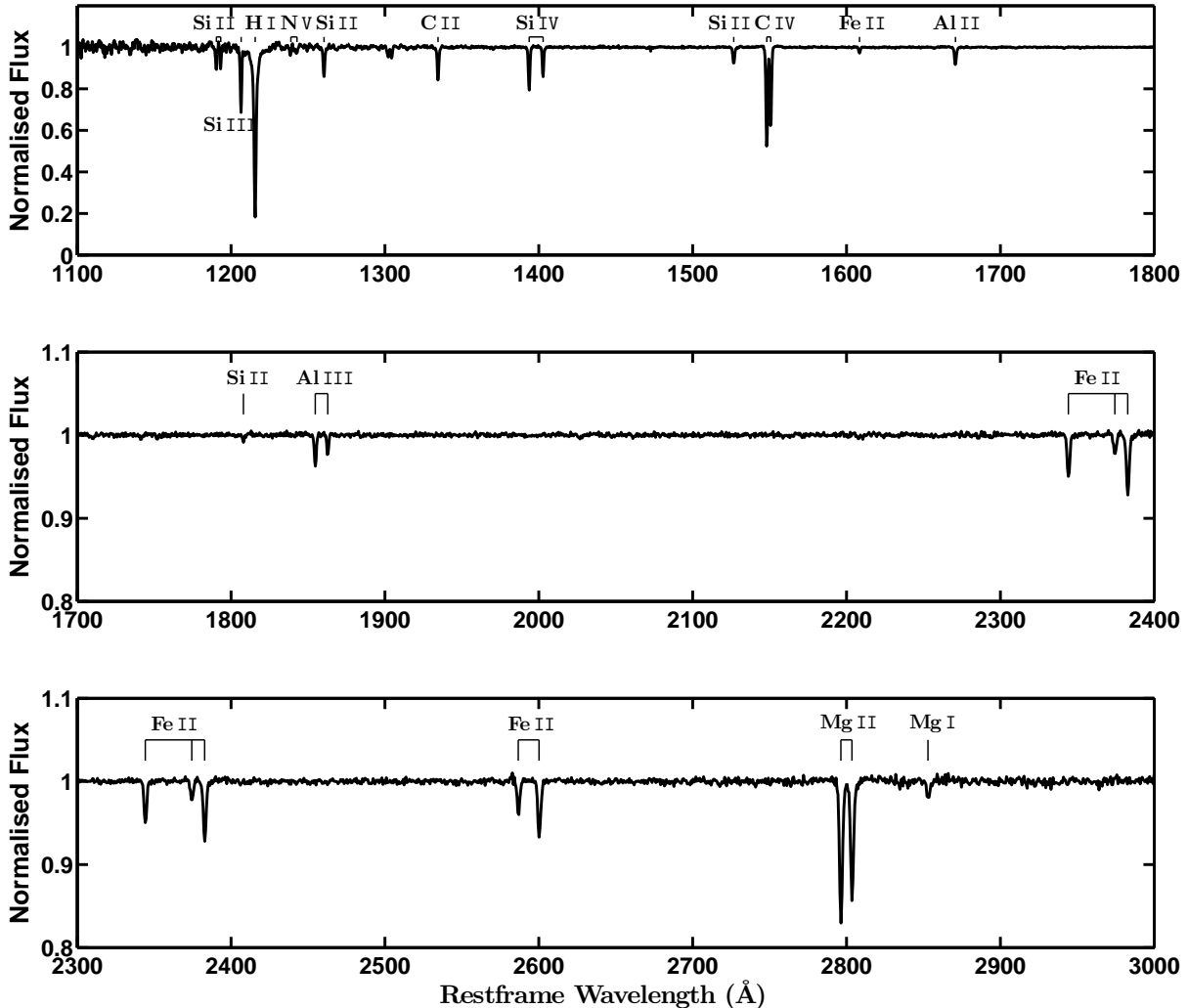


Figure 3. Arithmetic-mean composite absorption-line spectrum of 5098 C IV absorbers with $0.04 < \beta < 0.1$ identified in the non-BALQSO sample. The individual quasars containing the absorbers were normalised using a high S/N quasar composite (Section 5) and then combined in the rest-frame of the absorbers. The number of absorbers contributing to the composite decreases towards the wavelength extremes, causing the reduction in the S/N, but always exceeds 300 absorbers. The location of strong absorption lines are indicated, including features evident in later figures, e.g. the Fe II $\lambda 1608$ and Al II $\lambda 1671$ lines (see Fig. 4). Note the change in the y-axis range for the top panel.

3.3 Identifying triplet C IV absorbers

With the C IV-absorber sample in hand it is straightforward to search for potentially line-locked C IV systems via the distribution of separations from C IV-doublets to other (individual) absorbers blueward of the C IV doublet. The presence of line-locked C IV systems would lead to an excess of separations of absorbers at ≈ 14.5 pixels, indicating the presence of three, equally-spaced, absorption features, henceforth ‘triples’.

Figure 4 shows the distribution of C IV-doublet to absorber separations for C IV doublets with $0.05 < \beta < 0.10$ identified in the non-BALQSO sample. The separation is measured from the position of the blue (1548.19 \AA) line in each C IV doublet. The distribution is dominated by the 4579 pairs with separations of 7.24 ± 1.00 pixels; the C IV doublets themselves. At larger pixel-

lags ≈ 165 and ≈ 332 pixels), the detection of Fe II $\lambda 1608.5$ and Al II $\lambda 1670.8$ absorption respectively, associated with some of the C IV absorbers (see Fig. 3) demonstrates the effectiveness of the absorption-line identification scheme. Evidence for some line-locked C IV systems can be seen from the small, but significant, excess of $\approx 87 \pm 13$ absorbers around ≈ 14 pixels. The exact number of doublet-absorber pairs at larger separations depends primarily on the velocity-separations of the C IV doublets from the bulk of the outflow-related absorbers present at $\beta \lesssim 0.02$ in the quasars (Fig. 1). The broad excess of doublet-absorber detections centred at ~ 250 pixels results from the increased number of such pairs.

Considering the number of C IV doublet to absorber separations for doublets at smaller values of β reveals a clear detection of an excess of absorbers at ≈ 14.5 pixels, indicating the potential

presence of line-locked C IV systems in both the non-BALQSO and BALQSO samples. Figure 5 shows the histograms of C IV doublet to absorber separations for doublets with $0.0 < \beta < 0.05$ in the 31 142 non-BALQSO and 2654 BALQSO samples. Excesses of ≈ 800 (220) absorber-pairs at ≈ 14.5 pixels for the non-BALQSO (BALQSO) samples are present. The number of C IV doublets is much smaller in the BALQSO sample but no other significant excess of doublet-absorber pairs is evident at other velocity separations in either of the samples.

4 THE STATISTICS OF LINE-LOCKED SYSTEMS

4.1 C IV absorbers of different physical origin

The absorber-identification scheme described in the previous section, while effective, is essentially blind to the intrinsic nature of the absorber systems found. In addition to the outflowing absorbers that are the focus of the investigation, there are four additional sources of C IV doublets in the absorber catalogue: (a) spurious systems due to the limited S/N of the quasar spectra and hence of the absorber detections, (b) apparent C IV systems resulting from the presence of one, or two, real narrow Gaussian-like absorption features arising from species other than C IV, (c) real C IV absorbers due to intervening gaseous systems that are not directly related to the quasars but possess redshifts that apparently place them within $30\,000\text{ km s}^{-1}$ of the quasar redshift, (d) real C IV absorbers resulting from gaseous systems that are directly related to the presence of the quasar, e.g. within the quasar host-galaxy halo or associated with galaxies in the same group or cluster in which the quasar resides. The incidence of line-locking of interest is that relative to the proportion of C IV systems in outflows and a statistical correction to the observed number of absorbers is desirable for each of the four ‘contaminant’ populations.

The number of apparent C IV doublets, due to the coincidence of two spurious Gaussian absorbers with the velocity separation of a C IV doublet, was estimated by performing a search for Gaussian ‘emission’ features in the same quasar spectra (both the non-BALQSO and BALQSO samples). From the resulting catalogues of low S/N emission features, a total of 36 ± 2.5 and 16 ± 1.5 spurious C IV doublets were ‘identified’ per 0.01 interval in β for the non-BALQSO and BALQSO samples respectively. The expected number of C IV triple-systems resulting solely from the coincidence of three spurious absorber detections is essentially zero.

The majority of both C IV doublets and triplets that are not real arise from the coincidence of genuine, usually weak, absorption features present at the velocity separations used to define C IV doublets or triplets. The probability of finding a narrow Gaussian-like absorber at a given velocity separation from a location chosen at random within the quasar spectra is straightforward to determine empirically. Specifically, on average the probability is equal to 0.52 (0.76) per cent, per pixel, at small velocity separations ($\lesssim 1500\text{ km s}^{-1}$) for the non-BALQSOs (BALQSOs). Taking the sample of Gaussian absorbers in the non-BALQSO sample, there is therefore an approximately 1/200 chance that another Gaussian absorber will be found in a single pixel at a specified velocity separation. A C IV doublet was defined by requiring the presence of a second Gaussian absorber within ± 1.0 pixels of the predicted 500 km s^{-1} doublet separation and thus 1.04 (1.53) per cent of the C IV doublets are predicted to be spurious. It is worth noting that the contamination of the sample of C IV doublets due to effects arising from both the finite S/N of the spectra and the presence of

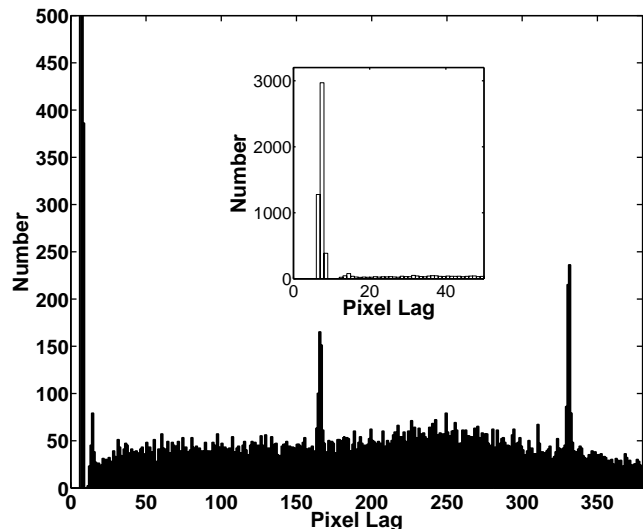


Figure 4. A histogram of the separation between the blueward trough of an identified C IV doublet, and all other identified individual absorbers in that quasar spectrum, for C IV doublets with $0.05 \leq \beta \leq 0.10$ (i.e. at velocities of $v_{\text{outflow}} > 15\,000\text{ km s}^{-1}$) identified in the 31 142 non-BALQSO sample. The distribution is dominated by the 4579 detections of the H1550.5 Å line in each doublet at 7.24 ± 1.00 pixels — i.e. the C IV doublets themselves (shown in the smaller enclosed plot). At larger pixel-lags, (≈ 165 and 332 pixels), the detection of Fe II λ 1608.5 and Al II λ 1670.8 absorption respectively, associated with some of the C IV doublets (see Fig. 3), demonstrates the effectiveness of the absorption-line identification scheme. Evidence for the presence of some line-locked C IV systems can be seen from the small, but significant, excess of ≈ 90 absorbers around ≈ 14 pixels.

unrelated absorbers (i.e. correction factors ‘a’ and ‘b’ above) is thus very small.

Triplet absorbers were defined by requiring the presence of a third Gaussian absorber within ± 1.5 pixels of the predicted location of a line-locked absorber associated with each C IV doublet⁵. The number of spurious triples is therefore equal to 1.52 (2.29) per cent of the number of C IV doublets identified in the non-BALQSO (BALQSO) samples. As a consequence, the correction to the observed number of triplet absorbers is fractionally quite large, particularly at small values of β , where the number of outflow C IV doublets is significant.

Potential higher-order systems, consisting of four or more absorbers separated by 7.24-pixels, were also sought. The number of spurious systems includes a component (exactly analogous to the calculation for the triplets) equal to 1.52 (2.29) per cent of the number of C IV triplets identified in the non-BALQSO (BALQSO) samples. In addition, the probability that two real C IV doublets, separated by 14.5-pixels, occur is not insignificant. Again, the number of such instances expected is readily calculated from the statistics of the number of C IV doublets identified per β -interval.

The number of intervening C IV absorbers present in the absorber catalogue was calculated using the results from Cooksey et al. (2013). For the EW_{1548} -interval $0.4 < \text{EW}_{1548} < 0.9$

⁵ The ± 1.5 pixel definition was determined from the observed velocity-width evident for absorbers associated with the C IV doublets, e.g. the Fe II λ 1608 and Al II λ 1671 lines in Fig 3, much of which results from the low S/N of the individual absorber detections. Other than the exact number of systems defined, none of the results in the paper are sensitive to the precise definition of doublets or triplets in velocity space.

Å, where the absorber sample is close to complete, the slope of the power-law model for the EW frequency distribution ($f(\text{EW}_{1548})$) of Cooksey et al. (2013), $f(\text{EW}_{1548}) = ke^{\alpha\text{EW}_{1548}}$, with $k=3.49$ and $\alpha=-2.62$, is in excellent agreement with the observed $f(\text{EW}_{1548})$ in the non-BALQSO sample. Calculating the redshift-path for detection of C IV absorbers in the 31 142 quasars of the non-BALQSO sample as a function of β produces a predicted number of intervening C IV absorbers. For the β -interval $0.05 \leq \beta \leq 0.10$, the Cooksey et al. (2013) model predicts 1329 ± 140 intervening absorbers, compared to the total of 2063 absorbers detected. Thus, 64.4 ± 8 per cent of the detected absorbers with $0.05 \leq \beta \leq 0.10$ are estimated to be intervening.

A correction for the number of intervening C IV absorbers for the full sample was made by assuming that the observed excess of associated systems in the $0.05 < \beta \leq 0.1$ interval is independent of absorber rest-frame EW_{1548} ; leading to a predicted number of intervening absorbers [in the full EW_{1548} -range] of 723 ± 58 (62 ± 5) per 0.01-interval in β for the entire non-BALQSO (BALQSO) sample. The EW_{1548} -extrapolation involved is small (≈ 80 per cent of the entire absorber sample possess $\text{EW}_{1548} \geq 0.3$ Å) and the key results reported below are insensitive to the exact level of the correction for intervening absorbers because the sample is dominated by outflowing absorbers at $\beta < 0.05$.

The same correction for the presence of intervening absorbers was applied to the BALQSO sample, taking into account the smaller total redshift path.

At small β values ($\beta < 0.01$) there is evidence (Fig. 1) for a population of ‘associated’-absorbers (‘d’ above) that do not participate in any outflow present. Without additional information it is not straightforward to derive an accurate estimate of the number of such associated-absorbers as a function of β . The exclusion of the $\beta < 0.00$ absorbers results in a very crude, partial, correction by removing absorbers that, given the level of the quasar redshift uncertainties, are unlikely to form part of any outflow. The statistics of the line-locked systems at small β values thus represent lower-limits to the fraction of such systems present in any outflows.

4.2 The fraction of line-locked C IV absorbers

Tables 1 (non-BALQSOs) and 2 (BALQSOs) include the observed and corrected numbers of C IV doublets and triplets as a function of β . The figures in Tables 1 and 2 for $\beta \leq 0.03$ demonstrate unambiguously that approximately 10 per cent of C IV absorbers associated with quasar outflows are line-locked. Given the very small number of individual line-locked absorber systems reported in the literature the result was not anticipated. Also of potential interest is the presence of line-locked narrow C IV absorbers in the BALQSO sample, with a frequency very similar to that in the non-BALQSO sample.

The observed number of quadruple systems, potentially representing three line-locked C IV doublets, is small. The majority are predicted to be due to chance occurrences of [non-line-locked] doublets, a conclusion that is confirmed via construction of composite absorber spectra (Section 5.3). The reality of the line-locked triplet systems is established explicitly in Section 5, but first the prevalence of line-locked absorbers in the subset of quasars where outflowing triplets can be detected is considered.

4.3 The fraction of quasar outflows with line-locked C IV absorbers

Line-locked C IV absorbers can only be detected in quasars where two or more C IV absorbers in an outflow are present. Given the frequency of C IV absorbers in the quasar samples, the majority of quasars possess only a single C IV absorber, which, in many cases, is due to an unrelated intervening absorber not associated with an outflow. Consideration of the statistics of line-locked systems in quasars with two or more C IV absorbers is revealing. Tables 3 and 4 present the number of absorbers present in the non-BALQSO and BALQSO samples, excluding quasars with only a single C IV doublet detected.

To investigate the frequency of line-locked systems it is necessary to define a velocity (i.e. β) interval in which two or more absorbers are detected, which in turn requires some knowledge of the extent of an outflow. In the limit of the velocity interval $\Delta\beta \rightarrow 0$, only line-locked systems (i.e. ‘triples’) will be included and the line-locked frequency will be ≈ 100 per cent. At the other extreme, using a very large velocity interval will lead to a sample dominated entirely by intervening doublet absorbers. Given the distribution of C IV absorbers as a function of β (Fig. 1), outflow extents of order $3000 - 10\,000 \text{ km s}^{-1}$ are an appropriate choice. Examining the β -range $\beta \leq 0.05$ ensures that a significant fraction of the absorbers are associated with outflows.

For completeness, Tables 3 and 4 include the statistics for β -intervals of 0.01 to 0.05, starting at $\beta=0.0$, along with the results for a 5000 km s^{-1} interval starting at $\beta=0.0067$ (i.e. 2000 km s^{-1}), chosen to focus on an outflow velocity range, some ten times the C IV line-locking scale (i.e. 500 km s^{-1}), that avoids the majority of the ‘associated’-absorbers [at small β] while minimising the fraction of intervening C IV absorbers.

Uncorrected and corrected figures for the number of quasars with multiple C IV absorbers and the number with line-locked triplet absorbers are included in the tables. The correction for the number of spurious triplets in each β -interval is straightforward to calculate using the numbers from columns 5 and 6 of Tables 1 and 2. The reduction in the number of quasars with multiple absorbers due to removal of the fraction of spurious triples is less than the loss of triples because some quasars possess two C IV doublets and a triplet. A statistical correction to the number of quasars with multiple absorbers due to the occurrence of a) two intervening C IV doublets and b) an intervening C IV doublet and a single C IV doublet in an outflow has also been applied. The probability that a quasar possesses an intervening absorber is known to high accuracy for each β -interval and the number of quasars with pairs of such absorbers is calculated assuming the absorbers are independent (i.e. there is no clustering; which, in practice, is a good approximation).

The number of C IV doublets resulting from outflows in each β -interval is also known to high accuracy. The correction for the presence of pairs of intervening and outflow C IV doublets is calculated assuming that both the intervening and outflow doublets are distributed randomly. The latter assumption is not exactly correct as at least some outflows will produce multiple C IV doublets in individual quasars. However, the distribution of outflow doublets, for all the β intervals, among the 31 142 non-BALQSOs is dominated by quasars with 0, 1 or 2 C IV doublets. For example, in the largest β -interval employed (0.00-0.05), i.e. worst-case, there are 7550 outflow C IV doublets in total, with 4431, 992 and 241 quasars possessing 1, 2 and >2 C IV doublets respectively. A significant fraction of the 241 quasars (≈ 150) are predicted to result from the presence of three intervening doublets or two interven-

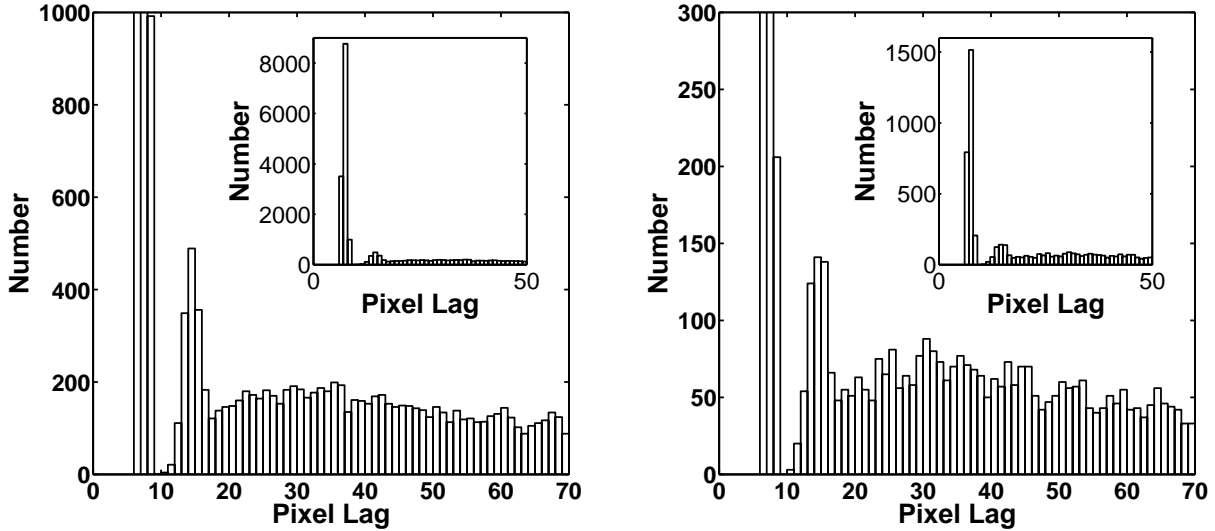


Figure 5. As for Fig. 4, histograms of the separation between the blueward trough of an identified C IV doublet, and all other identified individual absorbers in that quasar spectrum. Separations for absorbers with velocity $0.00 \leq \beta \leq 0.05$ identified in the 31 142 non-BALQSOs (left panel) and in the 2654 BALQSOs (right panel) are shown. The distribution is dominated by the $\approx 12\,000$ (1800) detections of the 1150.5 \AA line in each doublet at 7.24 ± 1.00 pixels for the non-BALQSOs (BALQSOs)— (shown in the smaller enclosed plots). The excess of ≈ 800 (220) absorber-pairs centred around 14.5 pixels provides clear evidence for a population of C IV triplet absorbers in the non-BALQSO (BALQSO) sample.

Table 1. C IV doublet and triplet systems in the non-BALQSO sample. Column 1 specifies the range in β and Column 2 gives the observed number of C IV doublets. The number of C IV doublets after correction for the number of spurious systems (i.e. factors ‘a’ and ‘b’ described in the text) is given in Column 3 and the number of C IV doublets after subtraction of the number of intervening systems, unrelated to the quasar (i.e. including factor ‘c’ described in the text) is given in Column 4. Columns 5 and 6 provide the observed and corrected number of C IV triplets (there are no intervening systems to be subtracted). Finally, Columns 7 and 8 provide the observed and corrected numbers of higher-order multiple C IV absorbers, i.e. quartets, quintets,...). The number of multiple absorbers with five or more components is small and the distribution is completely dominated by the number of quadruple absorbers.

β	N_{Obs}	Doublets		Triplets		Quadruplets+	
		$N_{Corr(ab)}$	$N_{Corr(abc)}$	N_{Obs}	$N_{Corr(ab)}$	N_{Obs}	$N_{Corr(ab)}$
0.00-0.01	4968 \pm 71	4873 \pm 71	4150 \pm 71	574 \pm 24	486 \pm 24	90 \pm 10	41 \pm 10
0.01-0.02	2301 \pm 48	2239 \pm 48	1516 \pm 48	163 \pm 13	124 \pm 13	41 \pm 7	27 \pm 7
0.02-0.03	1573 \pm 40	1520 \pm 40	797 \pm 40	73 \pm 9	47 \pm 9	6 \pm 3	1 \pm 3
0.03-0.04	1230 \pm 35	1182 \pm 35	469 \pm 35	41 \pm 6	21 \pm 6	4 \pm 2	0 \pm 2
0.04-0.05	1093 \pm 33	1047 \pm 33	371 \pm 33	22 \pm 5	5 \pm 5	4 \pm 2	2 \pm 2
0.050-0.075	2321 \pm 48	2219 \pm 48	666 \pm 48	68 \pm 8	31 \pm 8	5 \pm 2	-1 \pm 2
0.075-0.100	2111 \pm 46	2030 \pm 46	864 \pm 46	65 \pm 8	31 \pm 8	8 \pm 3	3 \pm 3

Table 2. C IV doublet and triplet systems in the BALQSO sample. Column definitions are as for Table 1

β	N_{Obs}	Doublets		Triplets		Quadruplets+	
		$N_{Corr(ab)}$	$N_{Corr(abc)}$	N_{Obs}	$N_{Corr(ab)}$	N_{Obs}	$N_{Corr(ab)}$
0.00-0.01	603 \pm 25	576 \pm 25	514 \pm 25	102 \pm 10	85 \pm 10	25 \pm 5	14 \pm 5
0.01-0.02	511 \pm 23	485 \pm 23	423 \pm 23	101 \pm 10	87 \pm 10	21 \pm 5	11 \pm 5
0.02-0.03	344 \pm 19	322 \pm 19	260 \pm 19	46 \pm 7	37 \pm 7	15 \pm 4	9 \pm 4
0.03-0.04	217 \pm 15	197 \pm 15	136 \pm 15	13 \pm 4	8 \pm 4	3 \pm 2	2 \pm 2
0.04-0.05	148 \pm 12	131 \pm 12	73 \pm 12	11 \pm 3	7 \pm 3	1 \pm 1	1 \pm 1
0.050-0.075	254 \pm 16	216 \pm 16	84 \pm 16	18 \pm 4	10 \pm 4	0 \pm 1	0 \pm 1
0.075-0.100	189 \pm 14	160 \pm 14	61 \pm 14	13 \pm 4	8 \pm 4	2 \pm 1	2 \pm 1

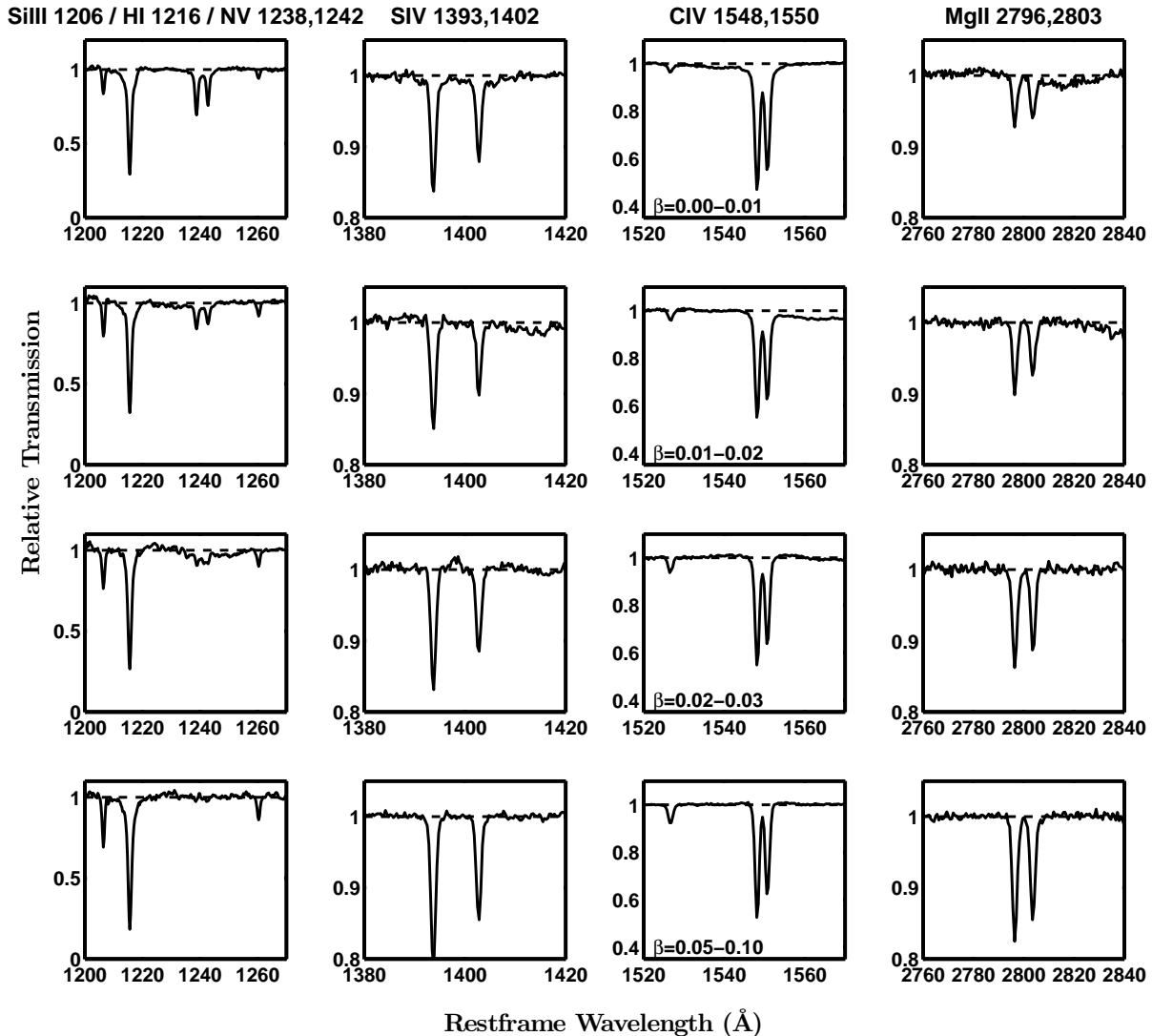


Figure 6. Arithmetic-mean composite absorption-line spectra of C IV doublets in quasars with only a single absorber. The signature of the quasar SED has been removed via the use of a composite quasar SED, as described in (Section 5). From left to right, the panels show four wavelength intervals containing strong absorption features. From top to bottom, the panels show the absorption-line spectra in intervals of increasing β , as specified in the panels of the third column. A strong systematic trend is present as a function of increasing β , with lower ionization species (e.g. Mg II) strengthening and higher ionization species (e.g. N V) weakening.

ing doublets and one outflow doublet, for which no correction has [deliberately] been applied. In summary, the corrected fractions of quasars exhibiting line-locked C IV absorbers are likely to be systematically too high but by an amount that is less than than the quoted errors (derived using counting statistics alone).

The statistics presented in Tables 3 and 4 represent key results of the investigation: approximately two thirds of quasars with multiple C IV absorption systems in outflows extending to $\sim 12000 \text{ km s}^{-1}$ possess line-locked C IV absorbers, visible as C IV absorber triplets. The line-locked absorbers are present in both non-BALQSO and BALQSO samples with comparable frequencies.

5 PROPERTIES OF LINE-LOCKED SYSTEMS

The low S/N of individual absorbers precludes their use to investigate any systematic change in properties as a function of β , or other parameters of interest. Information can be extracted using composite spectra of many absorbers but first it is necessary to isolate the absorption-line spectrum from the underlying quasar SEDs, which possess an extended range of properties. An effective solution is to construct a high-S/N composite quasar spectrum for each individual quasar that possesses an absorption system. The composite quasar spectrum can then be divided into the individual quasar spectrum, removing the ‘quasar signal’ and leaving the absorption-line spectrum alone. Groups of such absorption-line only spectra can then be combined to produce a high-S/N composite absorption-spectrum.

Table 3. Triplet systems in the non-BALQSO quasars with multiple C IV absorbers. The content of Tables 3 and 4 is as follows. Column 1; range in β . Column 2; number of quasars with multiple C IV absorbers. Column 3; total number of C IV doublets and triplet systems. Column 4; corrected number of quasars with multiple C IV absorbers after statistically removing pairs of intervening C IV doublets and pairs of intervening and outflow doublets. Column 5; the number of triplet-systems alone. Column 6; corrected number of triplet absorbers after allowing for the number of spurious systems (using the same correction scheme as in columns 5 and 6 of Tables 1 and 2. Column 7; percentage of quasars with multiple absorbers due to outflowing material that possess line-locked C IV absorbers.

β	N_{abs}	N_{quasar}	NC_{quasar}	N_{Trip}	NC_{Trip}	F_{Trip}
0.00-0.01	1115	819	617	572	484	78±5%
0.00-0.02	2299	1413	973	729	603	62±4%
0.00-0.03	3240	1850	1124	802	651	58±4%
0.00-0.04	3966	2165	1116	837	667	60±4%
0.00-0.05	4669	2460	1047	858	671	64±4%
0.0067-0.0233	939	607	393	328	276	70±6%

Table 4. Triplet systems in the BALQSO quasars with multiple C IV absorbers. Column definitions are as for Table 3.

β	N_{abs}	N_{quasar}	NC_{quasar}	N_{Trip}	NC_{Trip}	F_{Trip}
0.00-0.01	202	149	118	101	84	71±11%
0.00-0.02	647	382	309	194	164	53±7%
0.00-0.03	988	518	403	234	196	49±6%
0.00-0.04	1189	591	430	245	203	50±6%
0.00-0.05	1344	638	425	256	210	49±6%
0.0067-0.0233	431	269	216	161	135	63±8%

Quasars from the non-BALQSO sample (Section 2), without detected C IV absorption, were employed to provide a catalogue of ‘control quasars’, from which high-S/N composite quasars were generated. For each quasar with a detected C IV absorber (absorber quasar), the 100 quasars in the control sample with the closest absolute magnitudes, M_i , within $\Delta z \pm 0.1$ of the absorber quasar, are identified. Selection of quasars with very similar M_i minimises any systematic differences in emission line to continuum ratios (Baldwin 1977), while the narrow redshift interval maximises the rest-wavelength range in common with the absorber quasar. The quasars are normalised to possess the same integrated flux, using the rest-wavelength interval 1650-2250 Å. The normalised spectra are then combined, employing a simple arithmetic mean at each rest-wavelength, to produce a composite spectrum. The composite is normalised to the integrated flux of the absorber quasar and divided into the absorber quasar. The result is essentially a continuum-divided spectrum with the quasar signal removed and the absorption systems remaining. Small, large-scale, systematic differences in the slopes of the SEDs of the absorber and control quasars, consistent with the presence of dust at the level of $E(B - V) \simeq 0.01$ mag, associated with the absorbers or the quasars that possess absorbers, are still evident in the absorber composites. The implications for the dust content of the absorbers are discussed below (Section 5.2) but, to compare the absorber properties of the composites, any slope differences have been removed. Specifically, the composites have been normalised to unity using a large-scale median-filter derived continuum (filter-scale of 251 pixels, $\simeq 100$ Å).

5.1 Properties of the outflowing absorbers

Fig. 6 shows the results of the composite-absorber spectrum-generation scheme applied to the sample of quasars that possess only a single C IV doublet in the interval $0.0 \leq \beta \leq 0.1$. Composite

spectra are constructed as a function of β . The number of individual doublets is large, resulting in composites with a high S/N.

The single-doublet composite spectra are overplotted on the C IV-triplet composite spectra in Fig. 7. The figure demonstrates the reality of the line-locked systems unambiguously, through the presence of two absorber signatures (for multiple absorber species) separated by the 500 km s^{-1} C IV-doublet interval. Transitions resulting from hydrogen, magnesium, nitrogen and silicon are all present. The relative strengths of the twin absorption systems (see for example the Si IV $\lambda\lambda 1393, 1402$ panels) is consistent with the relatively low contamination of the observed C IV triplet sample, predicted from the statistics presented in Table 1.

Figure 8 shows the equivalent plot for the BALQSO sample. The large-scale depressions in the ‘continua’ evident in the figure are due to the presence of the extended BAL-troughs in the quasar spectra. Again, even with the poorer S/N, the signature of the twin absorption systems making up the C IV-triplets are clearly visible in the H I $\lambda 1216$, N V $\lambda\lambda 1238, 1242$ and Si IV $\lambda\lambda 1393, 1402$ transitions. The S/N for the Mg II $\lambda\lambda 2796, 2803$ absorption is particularly poor but even here, the presence of twin absorber systems can be made out at small β .

Figs. 7 and 8 provide a visual representation of some of the main results of the paper: i) a large fraction of intrinsically narrow ($\sigma \lesssim 200 \text{ km s}^{-1}$) absorption systems, present in outflows extending to at least $\gtrsim 20\,000 \text{ km s}^{-1}$, are line-locked, with velocity differences equivalent to the separation of the C IV $\lambda\lambda 1548.19, 1550.77$ absorption doublet, ii) the gas associated with the narrow absorption systems produces strong absorption due to species with a wide range of ionization potential (15.0 eV (Mg II) to 97.9 (N V) in Figs. 7 and 8), iii) line-locked absorption systems are present in both non-BALQSO and BALQSO samples and the dependence of the absorber properties as a function of outflow velocity, β , is similar.

The presence of species over an even greater ionization poten-

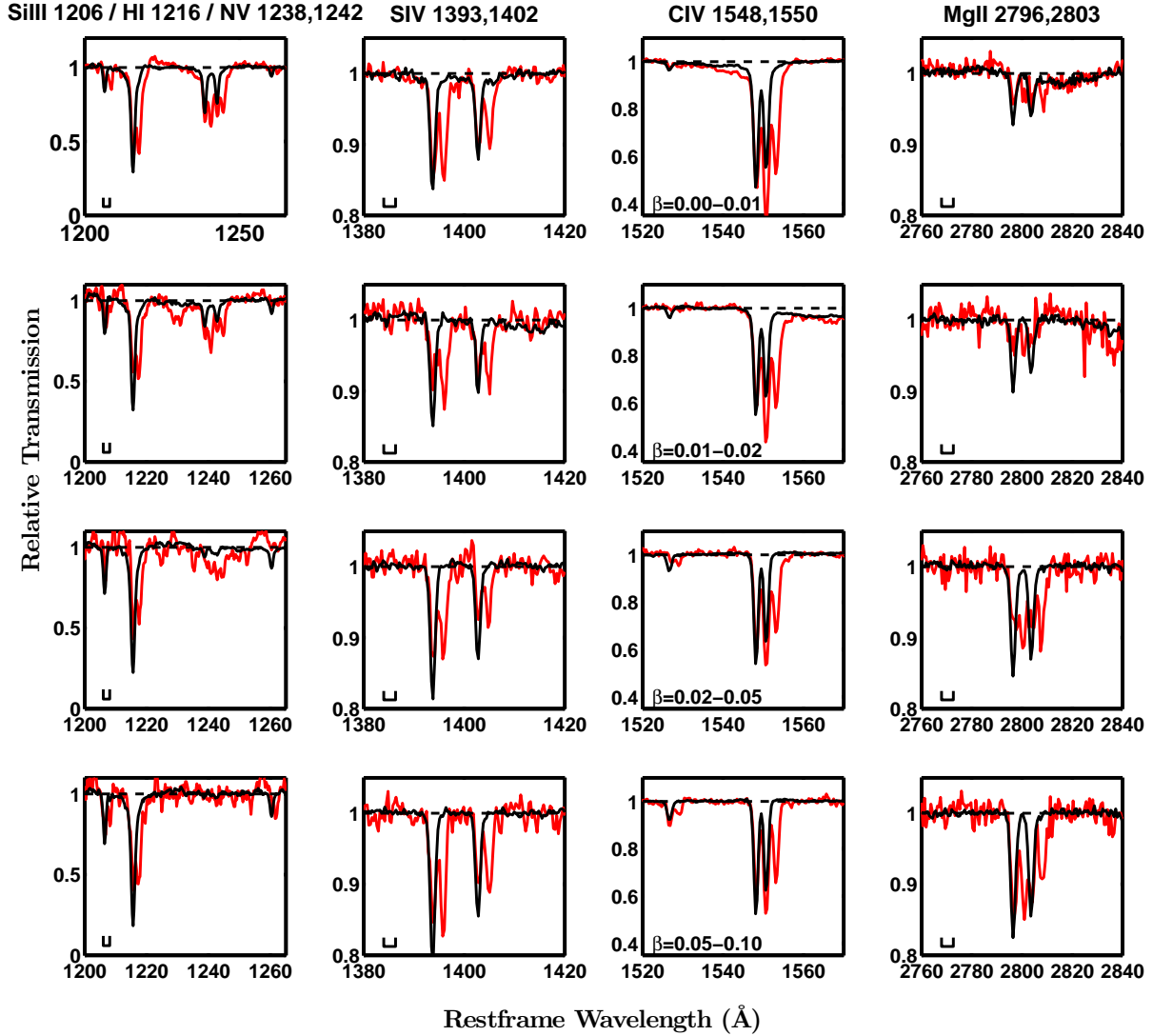


Figure 7. Arithmetic-mean composite absorption-line spectra of C IV triplet absorbers (red) with the composite absorption-line spectra of C IV doublets in the non-BALQSO sample with only a single absorber per quasar (c.f. Fig. 6) overplotted (black). From left to right, the panels show four wavelength intervals from each composite. From top to bottom, the panels show the absorption-line spectra in intervals of increasing β . The presence of ‘double’ H I, N V, Si IV and Mg II absorbers separated by the 500km s^{-1} interval (indicated by the lines in the bottom lefthand corner of each panel) resulting from two line-locked C IV systems demonstrates unambiguously the reality of the line-locked systems. The only slightly weaker EWs of the second absorber systems at redder wavelengths, (e.g. in Si IV and Mg II) confirms that the contamination of the C IV triplet sample due to spurious absorbers is small. The same systematic trend for species with different ionization potentials as a function of β is present for the line-locked systems and the C IV doublets.

Table 5. Absorption line ratios as a function of β for the non-BALQSO sample, derived from the composite spectra described in Section 5.

β	Single Doublets		Triplets	
	N V ₁₂₃₉ :C IV ₁₅₄₈	Mg II ₂₇₉₆ :C IV ₁₅₄₈	N V ₁₂₃₉ :C IV ₁₅₄₈	Mg II ₂₇₉₆ :C IV ₁₅₄₈
0.00-0.01	0.59 ± 0.05	0.11 ± 0.05	0.61 ± 0.05	0.13 ± 0.05
0.01-0.02	0.57 ± 0.05	0.22 ± 0.05	0.54 ± 0.05	0.25 ± 0.05
0.02-0.03	0.31 ± 0.05	0.42 ± 0.05	$<0.39 \pm 0.15$	0.39 ± 0.05
0.03-0.04	0.20 ± 0.05	0.73 ± 0.05	–	–
0.04-0.05	$<0.01 \pm 0.02$	0.57 ± 0.05	–	–
0.02-0.05	0.10 ± 0.05	0.63 ± 0.05	0.26 ± 0.10	0.59 ± 0.05
Intervening	$<0.01 \pm 0.02$	0.62 ± 0.05	–	–

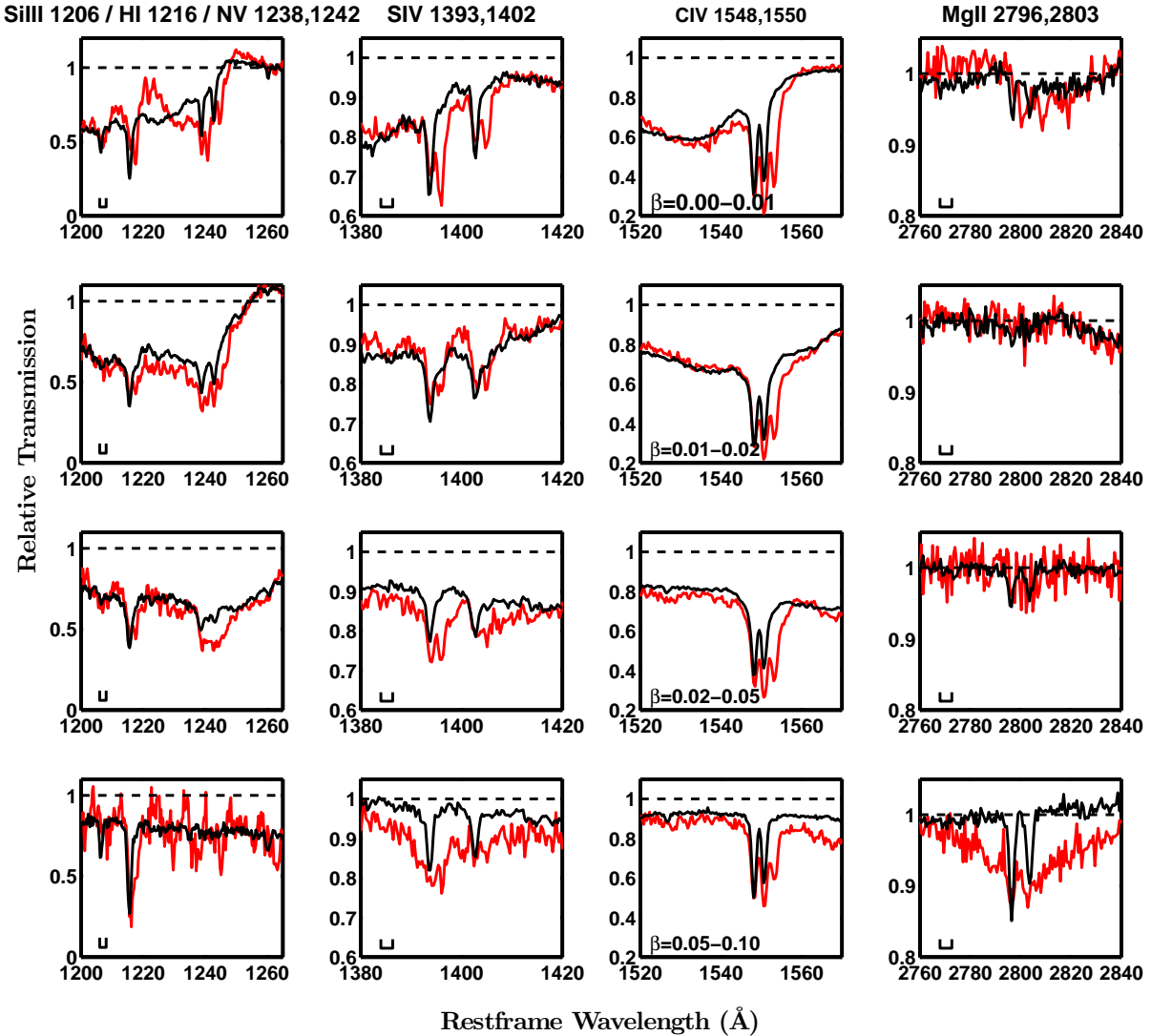


Figure 8. Arithmetic-mean composite absorption-line spectra of C IV triplet absorbers (red) with the composite absorption-line spectra of C IV doublets in the BALQSO sample with only a single absorber per quasar overplotted (black). From left to right, the panels show four wavelength intervals from each composite. From top to bottom, the panels show the absorption-line spectra in intervals of increasing β . The much smaller number of quasar spectra in the BALQSO sample means that the S/N of the composites is significantly poorer than for the non-BALQSO sample, particularly for Mg II and at large β , where the number of absorbers is small. The presence of ‘double’ H I, N V and Si IV absorbers separated by the 500km s^{-1} interval (indicated by the lines in the bottom lefthand corner of each panel) resulting from two line-locked C IV systems again demonstrates unambiguously the reality of the line-locked systems. The large-scale depression of the spectra, away from unit transmission, results from the presence of the extended BAL-troughs in the quasars [that are not present in the control-sample employed to remove the signature of the quasar SED]. The same systematic trend for species with different ionization potentials as a function of β , evident in the non-BALQSO sample, is present.

tial range is illustrated by the composite absorption-line spectra of C IV triplet absorbers and C IV doublets in the non-BALQSO sample where the absorber redshifts allow the rest-frame spectra to extend down to $\sim 1000\text{ \AA}$ (Fig. 9). The sample of 36 triplet absorbers and 448 doublet absorbers are from quasars with $2.8 \leq z \leq 3.0$, allowing the high-ionization O VI $\lambda\lambda 1031.9, 1037.6$ doublet (ionization potential 138 eV) to be included in the SDSS spectra. The S/N of the triplet-composite is not high but the presence of ‘double’ O VI, H I, N V and Si IV absorbers, separated by the 500km s^{-1} C IV-doublet interval confirms that the absorbers consist of gas, at ve-

locities coincident to $< 69\text{km s}^{-1}$ (i.e. one pixel in the SDSS spectra), with physical conditions capable of producing absorption due to species with a very extended range of ionization potentials.

The systematic trends in the properties of both the C IV doublet and triplet absorbers, notably the strength of the high- and low-ionization species as a function of β seen in Fig. 7, are quantified in Table 5. The ratio of the EW of N V₁₂₃₉ to C IV₁₅₄₈ decreases with increasing β , while that of Mg II₂₇₉₆ to C IV₁₅₄₈ increases. For the single C IV doublets, it is necessary to perform a correction

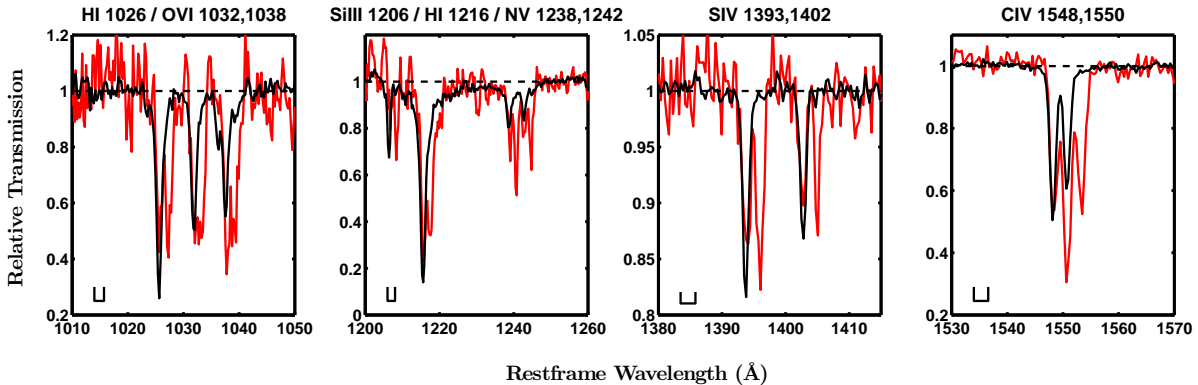


Figure 9. Arithmetic-mean composite absorption-line spectra of C IV triplet absorbers (red) with the composite absorption-line spectra of C IV doublets in the non-BALQSO sample overplotted (black). The sample of 36 triplet absorbers and 448 doublet absorbers are from quasars with $2.8 < z < 3.0$, where the high-ionization O VI $\lambda\lambda 1031.9, 1037.6$ doublet (ionization potential 138 eV) is visible in the SDSS spectra. The S/N of the triplet-composite is not high but the presence of ‘double’ O VI, HI, N and Si IV absorbers, separated by the 500 km s^{-1} C IV interval (indicated by the lines in the bottom lefthand corner of each panel), confirms that the absorbers consist of gas, at velocities coincident to $\leq 70 \text{ km s}^{-1}$, with physical conditions capable of producing absorption due to species with a very extended range of ionization potentials.

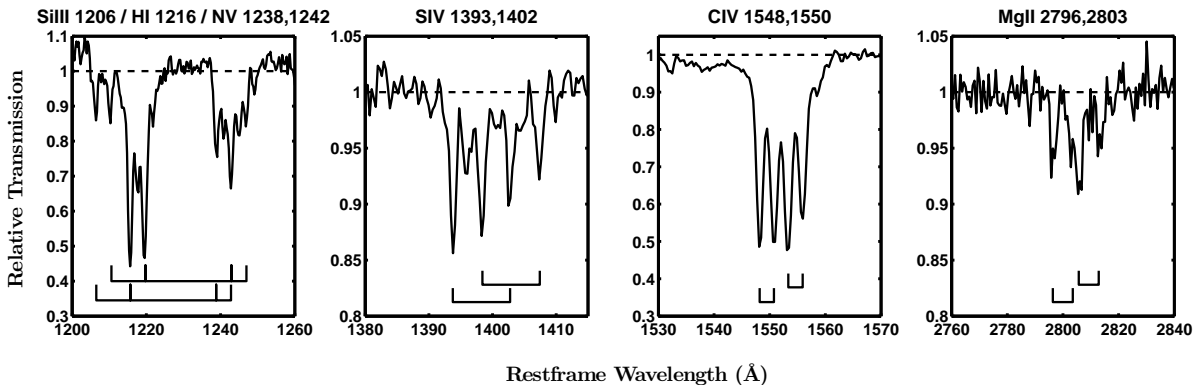


Figure 10. Arithmetic-mean composite absorption-line spectra of the 159 C IV quadruple absorbers (Table 1) in the non-BALQSO sample. The locations of absorption features assuming that the quadruples are made up of two C IV doublets, with no line-locking, are indicated by the bars at the bottom of each panel. The strong absorption features present for each species are consistent with the occurrence of two C IV doublets without any line-locking, in agreement with the statistics in Table 1. A fraction of the individual C IV absorbers are themselves almost certainly line-locked (producing a triplet signature in the other absorber species) as can be seen particularly in the Si IV panel and also with the weak fifth absorption feature redward of the four strong absorption dips in the C IV panel.

to the observed EW-ratios to allow for the presence of a significant number of intervening absorbers that are unrelated to outflows.

The EW-ratios for a composite spectrum constructed from a sample of 2200 C IV absorbers with $0.15 < \beta < 0.25$ were used to provide the values for intervening absorption systems. The EW-ratios for the single C IV-doublet absorber-composite in the interval $0.05 < \beta \leq 0.10$ are indistinguishable from the intervening absorber-composite, as expected, given intervening absorbers dominate the sample of single doublets at $\beta > 0.05$. Estimates of the Mg II:C IV and N V:C IV EW-ratios in the single C IV outflowing absorbers as a function of β are given in Table 5. The calculation assumes that the fraction of intervening single doublet absorbers in each β interval is given by the predicted numbers from Section 4.1, after the statistical removal of the number of quasars with multiple intervening absorbers and intervening plus outflow absorbers that contribute to the multiple-doublet sample (Table 3). For $\beta > 0.03$ the S/N of the triplet-absorber composites is very low and results for the larger interval $0.02 < \beta \leq 0.05$ are also given.

The systematic changes in the Mg II:C IV and N V:C IV EW-ratios as a function of β for the single-doublet and triplet absorbers in the outflows are consistent within the errors. The uncertainties in the EW-ratios for all but the very weak N V-absorption at large β are dominated by uncertainties in the exact placement of the ‘continua’, necessary for the measurements. The poor S/N in the absorber-composites for the BALQSO-sample precludes a similar quantitative comparison but inspection of Fig. 8 suggests that the same trends as seen in the non-BALQSO sample are present⁶.

⁶ The number of quasars with multiple C IV absorbers in the $\Delta\beta=0.01$ intervals (for both the non-BALQSO and BALQSO samples), even before correction for the fraction of intervening absorbers, is too small to provide significant constraints on the EW-ratio trends as a function of β , although the low-S/N composites are consistent with the results for the single absorbers and the triplets.

5.2 The SEDs of the host quasars

5.2.1 The dust content of the absorbers

Interpretation of any differences in the overall shape of the ultraviolet SEDs of the quasars with and without outflowing C IV absorbers is not straightforward, given the presence of populations of both associated and intervening absorbers in the same quasars. To test for the presence of dust associated with the outflow absorbers, composite host-quasar spectra were constructed for samples of triplet and single doublet absorbers in the non-BALQSO sample that lie in the interval $0.0067 < \beta < 0.0233$ (i.e. $2000\text{--}7000\text{ km s}^{-1}$, where few ‘associated’-absorbers are present). A large sample of quasars, with the same redshift and absolute magnitude distribution, from the sample of quasars with no detected C IV absorbers was used to provide the ‘control’ SED. Dividing each absorber-composite by the control-composite and fitting the resulting ratio (over the wavelength interval $1600\text{--}3300 \text{ \AA}$) with an SMC-like extinction curve gives $E(B - V) = 0.008 \pm 0.002$ and 0.016 ± 0.003 for the doublet- and triplet-composites respectively. The uncertainties are dominated by the intrinsic dispersion among the constituent quasar SEDs. The measurements are consistent with absorbers in the specified outflow velocity-range possessing a small dust content and the triplet sample consisting of pairs of such doublets.

The result strongly suggests that dust associated with the outflow absorbers is responsible for the small differences in the slope of the quasar ultraviolet SEDs but the interpretation is not unambiguous.

5.2.2 Differences in the intrinsic SEDs of the host quasars

Baskin, Laor, & Hamann (2013) investigated BALQSO ultraviolet SEDs and correlations with the high-ionization absorption properties, including outflow-velocity, β . Baskin, Laor, & Hamann (2013) draw particular attention to the anti-correlation between the strength of the He II $\lambda 1640$ recombination emission feature in the quasar spectra and the increasing β to which the BAL-troughs extend. The strength of He II is a measure of the far-ultraviolet quasar SED (capable of ionizing helium). A strong far-ultraviolet SED in the quasars results in highly ionized outflowing material and line-driven acceleration (e.g. via C IV) is thus reduced. As a consequence, material does not reach as extreme outflow velocities as in outflows associated with quasars possessing weaker far-ultraviolet SEDs.

Quantifying the EW of the relatively weak He II $\lambda 1640$ emission line is difficult. As described in their section 2, Baskin, Laor, & Hamann (2013) choose to define a continuum by extrapolating from a point redward (at 1720 \AA) of He II, producing EW-values of up to 10 \AA . Variations in the overall shape of the quasar SED also result in some dispersion in the inferred He II EWs.

The continuum-definition procedure is very different from that often employed, which results in He II-EW measurements of $\simeq 0.5 \text{ \AA}$, a factor of ten smaller (e.g. Vanden Berk et al. 2001). We have adopted the more traditional continuum-definition scheme, using a linear interpolation between the continuum levels at 1620 \AA and 1650 \AA . The He II-EW in composite spectra made from samples of $\simeq 1000$ quasars from the no-absorber non-BALQSO control sample is $0.62 \pm 0.01 \text{ \AA}$. Dividing the absorber sample at $\beta = 0.02$, to define ‘close’ ($< 6000 \text{ km s}^{-1}$) and ‘far’ ($> 6000 \text{ km s}^{-1}$) absorption, produces sub-samples of single doublet (sd), multiple doublet (md) and triplet (t) absorbers that produce composite quasar spec-

tra with adequate S/N to measure the relative He II-emission line strength to high accuracy.

The EW measurements for the close/far composites in the sd, md and t samples are $0.70/0.57$, $0.60/0.44$, $0.71/0.44 \text{ \AA}$ respectively. The continuum-definition procedure is well-defined and identical for each composite spectrum. The ratios of the EWs in the close to far samples are determined to an accuracy of better than 10 per cent and the three close/far ratios, of 1.23, 1.36 and 1.61, in the same sense (stronger He II-EW for absorbers with relatively low outflow velocities) as that determined by Baskin, Laor, & Hamann (2013) is potentially significant. The caveat is that the dominant uncertainties on the ratios for the md and t samples is the small number of quasars in the ‘far’-sub-samples and a more robust measurement is required to establish the systematic EW-difference definitively.

5.2.3 Differences in the global properties of the host quasars

Shen et al. (2011) provide a compilation of quasar properties for the SDSS DR7 quasars, including radio detections and estimates of the quasar luminosity relative to the Eddington luminosity. The non-BALQSO quasar sample can be divided into sub-populations with i) no C IV absorbers, ii) outflow absorbers, iii) line-locked outflow absorbers. While there are some weak trends that derive from the detectability of absorbers as a function of the S/N in the SDSS spectra, there are no significant differences among the sub-populations in a) radio-detection fraction, b) quasar luminosity or c) luminosity relative to the Eddington luminosity.

Given that a substantial fraction of all quasars show evidence for outflows (e.g. Ganguly & Brotherton 2008) and that such a large fraction of quasars with outflows show evidence for the presence of line-locked absorbers, the lack of significant differences in the distribution of such properties is perhaps not surprising.

5.3 Constraints on other line-locked absorber species

The focus of the investigation has been the presence of absorbers line-locked at the 500 km s^{-1} separation of the C IV $\lambda\lambda 1548, 1550$ doublet. The absorber detection procedure described in Section 3 requires absorbers to exhibit significant C IV absorption but the ‘triplet’-identification scheme is sensitive to any excess of C IV doublets present at line-locked velocity separations of other absorption species, e.g. N V $\lambda\lambda 1238, 1242$ (962 km s^{-1}) or Si IV $\lambda\lambda 1393, 1402$ (1932 km s^{-1}). Inspection of Fig. 4 and Fig. 5 demonstrates that no additional excess of absorber pairs is detectable at any separation [that can’t be attributed to pairs from different species in the same absorber system, such as the Al II and Fe II features seen in Fig. 4].

In fact, the C IV doublet catalogue does not provide much sensitivity to the detection of C IV doublets line-locked at velocity separations $\gtrsim 1100 \text{ km s}^{-1}$ because there are so few quasars that possess pairs of C IV doublets that are separated by such velocities within individual outflows. Specifically, within the β -range $0.0 < \beta < 0.04$ there are only 1543 C IV doublet outflow-pairs with velocity separations $> 1100 \text{ km s}^{-1}$. Almost exactly two-thirds of the pairs are due to intervening-outflow absorber and intervening-intervening absorber coincidences, leaving just $\simeq 500$ C IV doublet outflow-pairs. As a result, to be detectable, a line-lock at a velocity $> 1100 \text{ km s}^{-1}$ in the non-BALQSO sample would have to include $\simeq 50$ per cent of the C IV doublet pairs at a given velocity. No evidence for any such line-locks is seen.

The number of C IV doublets present at separations where

line-locking due to N V $\lambda\lambda 1238, 1242$ at 962 km s^{-1} occurs is larger. The velocity separation is only half an SDSS-spectrum pixel different from the velocity separation of any trios of line-locked C IV doublets. The confusion with pairs of C IV doublets separated by $\simeq 500 \text{ km s}^{-1}$ and a small fraction of genuine quadruples due to three line-locked C IV doublets (Fig. 10) is such that, again, the constraint on the fraction of line-locked N V doublets is weak.

Information on the presence of other line-locked C IV doublet pairs will improve when larger samples of absorbers are analysed (e.g. the SDSS III quasar samples) but from the SDSS DR7 spectra the constraints on the prevalence of line-locking at $> 1100 \text{ km s}^{-1}$ are weak.

6 DISCUSSION

The presence of line-locked narrow C IV absorbers in the majority of highly ionized outflows associated with luminous quasars will likely provide powerful constraints on the acceleration mechanism responsible for the outflows and the physical conditions present in the flows. A detailed investigation of models is beyond the scope of this paper but some initial calculations, intended to illustrate several concepts, are presented below. The intention is not to attempt to model any particular outflow clouds in detail, a task that will be addressed in subsequent papers by exploring an extensive parameter space.

The radiative acceleration is given by (Castor 1974)

$$a_{\text{rad}} = \int_0^{\infty} \frac{4\pi F_{\nu}}{h\nu} \frac{\kappa_{\nu}}{\rho} \frac{1}{c} d\nu \quad (1)$$

where κ_{ν} is the gas opacity per nucleon, ρ is the mean density per nucleon, and the integral is over the incident radiation field F_{ν} . The gas opacity κ_{ν} is related to the optical depth, τ_{ν} , which we use throughout because it is directly observed, by

$$\tau_{\nu} = \int n \kappa_{\nu} dr \quad (2)$$

where n is the nucleon density and r is the cloud depth along the line of sight. In practice, the clouds considered below are fairly homogeneous, so τ_{ν} and κ_{ν} are nearly proportional to one another.

Two dependencies are revealed by equation 1. First, the metallicity Z enters through the ratio κ_{ν}/ρ because heavy elements provide most of the opacity but little of the mass - this ratio is proportional to Z . We assume conventional metallicities and do not explore consequences of changing Z in this paper. Second, the SED of the AGN enters through F_{ν} . We assume that the ratio $4\pi F_{\nu}/h\nu$ is constant as a first approximation although other SEDs are considered in Section 6.4.1.

6.1 Baseline C IV clouds

Version 13.03 of CLOUDY, most recently described by Ferland et al. (2013), is employed to simulate conditions within clouds. The results given in table 3 of Hamann et al. (2011) are used as a guide to set up a simple baseline photoionization model. It is assumed that the cloud is irradiated by the standard active galactic nuclei (AGN) SED built into CLOUDY.

Gas found near the centres of AGN, or massive galaxies generally, has metallicities significantly above solar (Hamann & Ferland 1999). Therefore, adopting a conservative approach, metallicity, Z , is set at three times higher than solar. In practice, the default solar abundance for all elements heavier than helium is increased by a

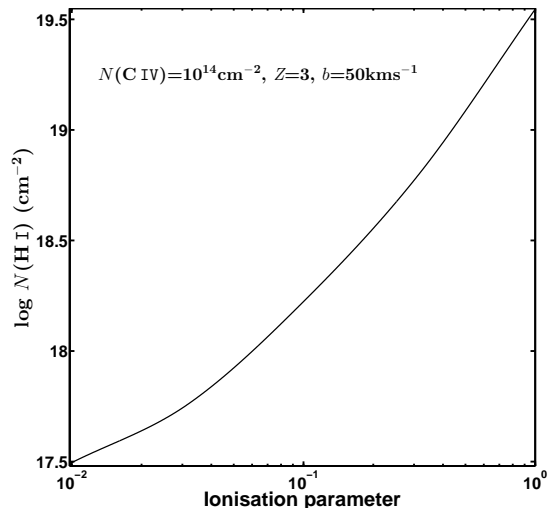


Figure 11. The total hydrogen column density $N(\text{H})$ is shown as a function of the dimensionless ionization parameter U . Enhanced abundances, a typical AGN SED, and a microturbulent velocity of 50 km s^{-1} were assumed. The measured reddening of 0.008 mag/cloud suggests $\log U \sim -0.3$

factor of three, with nitrogen increased by a further factor of three to account for secondary nitrogen production.

A representative column density of $N(\text{C IV}) = 10^{14} \text{ cm}^{-2}$ and a microturbulent velocity of 50 km s^{-1} are assumed, along with a hydrogen density of 10^5 cm^{-3} . This turbulence is supersonic with a Mach number of $\simeq 4$, meaning that turbulent pressure will dominate over gas pressure. These parameters are typical of the structures studied in Hamann et al. (2011) and produce an optical depth in the C IV doublet of a few, close to the observed value and optimised to produce the maximum acceleration due to C IV. The cloud is roughly isothermal with a temperature of $T \sim 20\,000 \text{ K}$, a typical value.

6.2 Hydrogen column density and cloud reddening

Photoionization simulations of the absorbers cannot determine the density of the cloud, only its ionization parameter U (i.e. the number of ionizing photons per atom). The results above (Section 5.2.1) suggest that each cloud has an internal reddening of $E(B-V) \approx 0.008 \text{ mag}$. The grain optical properties, the ratio of total to selective extinction R , and the dust to gas ratio, are unknown. Savage & Sembach (1991) find

$$\frac{N(\text{H})}{E(B-V)} = 5 \times 10^{21} \text{ cm}^{-2} \text{ mag}^{-1}. \quad (3)$$

to be typical within our Galaxy. If the dust to gas ratio scales with the metallicity Z , then the hydrogen column density corresponding to the deduced reddening is

$$N(\text{H}) = 4 \times 10^{19} \text{ cm}^{-2} Z^{-1} \quad (4)$$

A series of models are computed, where the ionization parameter, U , varies and the cloud thickness is adjusted to keep $N(\text{C IV}) = 10^{14} \text{ cm}^{-2}$. Figure 11 shows the total hydrogen column density as a function of U .

The deduced reddening and assumed grain properties correspond to $\log U \sim -0.3$ for $Z=3$. We adopt this abundance and value of U in the following work.

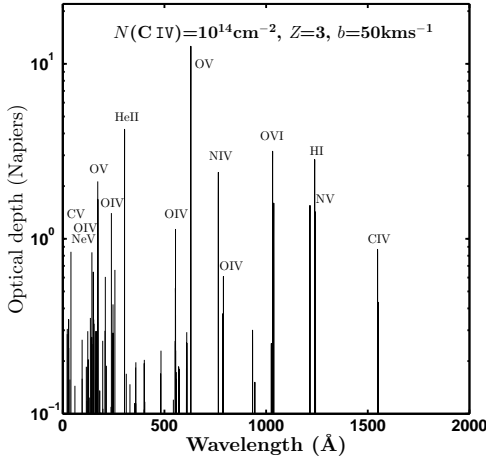


Figure 12. The line optical depths of the fiducial model are shown. The gas is fairly highly ionized, with most elements having four to six electrons removed, and the resulting permitted lines are mainly in the extreme ultraviolet. The very shortest wavelength lines are inner-shell transitions. The C IV doublet components are the longest-wavelength lines. The lines indicated at the shortest, very crowded, wavelengths are C V λ 40, Ne v λ 143, O IV λ 150 and O v λ 172.

6.3 Line optical depths for the fiducial cloud

CLOUDY includes a high-resolution fine opacity grid that is used for multi-grid calculations of line acceleration and overlap (Ferland et al. 2013). The predicted line optical depths in this fine grid are shown in Fig. 12.

Individual lines are well resolved on this fine grid, which has $R \equiv \lambda/\delta\lambda \sim 10^4$. In a highly ionized gas with enhanced abundances, the largest opacities are due to resonance lines of Li-like, He-like and H-like ions of O, C and N. The He II and H I resonance lines are also significant. There are an especially large number of lines at short wavelengths, $\leq 300\text{\AA}$. The lines grow sparser at longer wavelengths and the C IV doublet is the longest-wavelength feature. The details of the model do not affect these qualitative features.

6.4 The line autocorrelation signature

Clouds will tend to be accelerated up to line-locked velocities if line radiative acceleration is the dominant force acting on the clouds, and if the mutual self-shielding of overlapping strong lines produces a local minimum in the acceleration. The easiest way to search for such overlaps is by computing the line optical-depth autocorrelation function (ACF). The optimal situation for line-driven radiative acceleration is when the clouds possess an optical depth, τ_ν , of order unity for the line species. The momentum transfer from a line species essentially saturates once the optical depth is a few (there are hardly any photons remaining to be absorbed) and before calculating the ACF a ceiling of $\tau_\nu = 2$ was applied to the line optical depths shown in Fig. 12. The results of an autocorrelation analysis of the opacity distribution, is shown in the top panel of Fig. 13.

The autocorrelation results shown extend to velocity-separations of $\sim 7000\text{ km s}^{-1}$ and, as discussed in Section 5.3, the observational constraints on the presence of line-locks at separations $\gtrsim 1000\text{ km s}^{-1}$ are poor. That said, the form of the

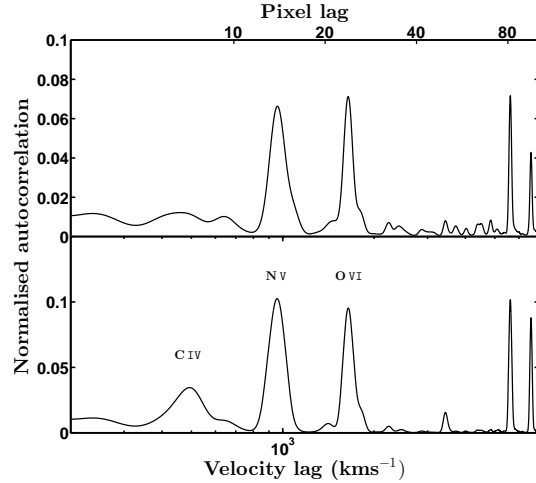


Figure 13. The line optical depth autocorrelation function is shown for the fiducial model. The top panel shows results for the lines shown in Fig. 12 with a maximum optical depth of $\tau=2$. The lower panel shows the autocorrelation for the same lines but weighted by the $v^{-0.7}$ factor, approximating the form of the incident AGN SED (see Section 6.4.1); the C IV doublet becomes the strongest feature below $\approx 1000\text{ km s}^{-1}$. The positions of the strong C IV, N V, and O VI doublet pairs are indicated in the lower panel. The ACFs are normalised such that they have a value of unity at zero-velocity and the features of interest are the relative heights of the peaks at velocities greater than 200 km s^{-1} (the minimum velocity shown on the x-axis above). The axis at the top shows the pixel-lag, to allow direct comparison with the observational data shown in Figs. 4 and 5.

ACF at lower velocities is not initially encouraging, as the 500 km s^{-1} signal due to the C IV doublet is immersed among a number of other line-lock signatures with similar velocities, due primarily to line species in the far ultraviolet part of the AGN SED.

For reasons related to the finite resolution of the SDSS-spectra and the velocity-separation of the C IV doublet (Section 3) identification of clouds with detectable C IV doublets, line-locked at separations $< 500\text{ km s}^{-1}$ is not possible. At velocities $> 500\text{ km s}^{-1}$ however, there is no reason why pairs of C IV doublets would not be found with velocity separations in the range $500\text{--}1000\text{ km s}^{-1}$. Such pairs would manifest themselves as an excess number of absorber detections above the background for pixel lags $\approx 15\text{--}30$ in the left-hand panel of Fig. 5. Any such population present is clearly at a much lower incidence than is the case for absorbers line-locked at the C IV doublet separation. The well-defined narrow peak of the third C IV absorption component evident in Fig. 5 and the essentially identical velocity-widths of the two intrinsic components making up each C IV line-locked triplet (Fig. 7) also provide evidence against the presence of a significant population of additional line-locked C IV absorbers with velocity separations $500\text{--}1000\text{ km s}^{-1}$. In principle, other line-pairings, with velocity separations of $\approx 500\text{ km s}^{-1}$, could be contributing to the peak at 500 km s^{-1} that we have ascribed to C IV. Removing the C IV doublet from the absorption-line opacity table, however, demonstrates that C IV dominates the contribution to the 500 km s^{-1} peak completely. A focus on factors that result in an enhanced C IV doublet signal, consistent with the observations, therefore appears worthwhile.

6.4.1 Changing the AGN SED Shape

The analysis above assumes a uniform weighting of the lines, ignoring the shape of the incident AGN SED responsible for accelerating the gas.

The SED used to compute Figs. 12 and 13 (top panel) is a generic AGN SED, deduced in part from observations of intrinsic emission lines. The SED that drives the absorbing clouds may not be the same. The central regions of an AGN are believed to have a cylindrical geometry with the emitting clouds along the equator. It is likely that we are viewing the AGN from regions near the axis of the cylinder since we have a relatively unobstructed view of the SED.

To examine the effects of various SEDs upon the auto correlation function the SED may be parametrized as a single power-law. The approach is only valid in the broadest sense, but has the advantage of simplicity and serves to show the dependencies of the ACF on the illuminating SED.

Assume therefore, that the AGN SED can be fitted, over the wavelength range shown in Fig. 12, with a power-law as a function of frequency, ν , $f_\nu \propto \nu^\alpha$. The photon-number flux is then $n_\nu \propto \nu^{(\alpha-1)}$. Assume further that lines are microturbulently broadened to a velocity width du (50 km s^{-1} is adopted in the baseline model). The line width in frequency units is $\delta\nu = du\nu/c$, where c is the velocity of light, and the number of photons within an absorption line is $n_{line} = n_\nu \delta\nu \propto \nu^\alpha$. Each photon has momentum $h\nu/c$, so the photon momentum transferred to the clouds is $\propto n_{line} h\nu/c \propto \nu^{\alpha+1}$.

The main effect of varying the slope of the SED is to change the weighting given to lines at different wavelengths. Steep slopes give greater weight to lines at longer wavelength. We adopt a power-law index of $\alpha = -1.7$, typical for the SDSS-quasars in the sample (e.g. Kruczek et al. 2011). The optical depths shown in Fig. 12 were rescaled by a factor $\propto \lambda^{0.7}$ and normalised to give a maximum optical-depth of $\tau = 2$ for the C IV 1548 Å line. The C IV doublet optical depth for the sample has to be of this order for the lines to be detected.

The resulting ACF is shown in the lower panel of Fig. 13. The steeper AGN SED results in the long-wavelength line pairs, due to O VI, N V and C IV, becoming stronger. In particular, the differences at velocities $\lesssim 1000 \text{ km s}^{-1}$, compared to the unweighted case, are significant and the peak due to the C IV doublet line-lock is much more pronounced and more consistent with the observations.

Future work should investigate how the ACF depends on the SED. Sophisticated AGN SEDs including the effects of a range in $L/L(\text{Edd})$ now exist (Jin et al. 2012). These could be combined with the ACF approach taken in this paper to investigate how the properties of the outflow depend on other AGN parameters.

6.5 Radiative acceleration and cloud stability

Line radiative acceleration must be important if line locking is to occur. Our CLOUDY calculations include a self-consistent treatment of acceleration by both lines and continua (Ferland et al. 2013). Line self-shielding and overlap with other lines is fully treated using the fine opacity grid shown in Fig. 12.

The database CLOUDY employs for resonance lines (transitions arising from the ground state) should be fairly complete and such transitions dominate the line-dependent acceleration. The situation contrasts with that applying to stellar winds where Castor, Abbott, & Klein (1975) stressed that millions of lines arising between excited states can contribute to the acceleration in a

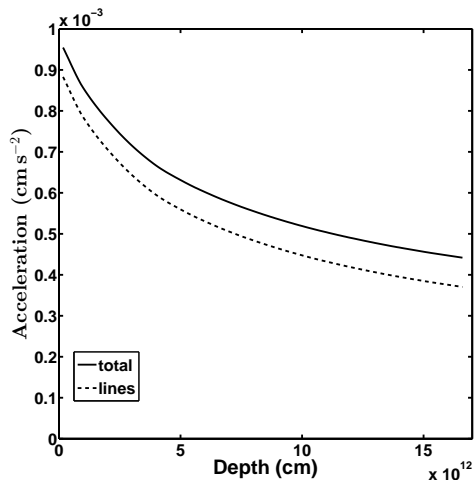


Figure 14. The radiative acceleration as a function of cloud depth for the fiducial model. The total- and line-only accelerations are the upper and lower curves respectively.

stellar atmosphere. This is not the case in the low density AGN absorber material considered here, where most atoms will be in the ground state. In an O-star wind, collisional processes resulting from the high densities create a substantial population of atoms in excited states, so subordinate lines (transitions between two excited states) are important. There are *many* more permitted subordinate lines, which are included in the CLOUDY calculations, but their influence is found to be unimportant. Fig. 12 shows all lines with significant optical depth.

Fig. 14 shows the acceleration across the fiducial cloud. The upper curve shows the total radiative acceleration while the lower curve includes only lines. The radiative acceleration is predominantly due to lines across the entire cloud. The acceleration is greatest at the illuminated face of the cloud, a depth of zero. The acceleration decreases as lines become optically thick and are self-shielded. As shown by Castor (1974, equation 3.48), the radiative acceleration decreases when the line optical depth becomes significant. The outward acceleration has fallen by about a factor of two at the shielded face of the cloud.

Although lines contribute 89 per cent of the total radiative acceleration, the C IV doublet is not an important contributor to this total. The O V $\lambda 629.7$ line contributes over two thirds of the total acceleration, with lesser contributors from the O VI and N V doublets. The C IV doublet contributes only about 1 per cent of the total. Nearly all of the acceleration due to continuum absorption is due to photoelectric opacity, with electron scattering being negligible.

The exploratory investigation has been successful in showing that line-driving is capable of accelerating ‘clouds’ with properties given in Section 6.1. In the context of the observations, it has also been possible to show that the line-locking signature due to C IV exists as a local maximum in velocity space. In terms of the spectrum of potential line-locks, the 500 km s^{-1} feature represents the lowest velocity feature present and the idea that material in an outflow might ‘lock’ naturally at the first significant peak in the line autocorrelation function (Fig. 13; lower panel) is attractive. What remains unclear, however, is why material in outflows appears to maintain the 500 km s^{-1} separation when the contribution

of the C IV-doublet represents such a small fraction of the total acceleration.

Line-driven winds are famously unstable (Owocki, Castor, & Rybicki 1988). The decreasing acceleration means that the cloud will be compressed, becoming a pancake (Mathews 1982). Eventually, the the geometry shown in Fig. 14 will become Rayleigh-Taylor unstable and will fragment over scales similar to the line shielding length. This brings in rich dynamical aspects which merit further more detailed investigation.

Fig. 14 gives hints to the origin of the line locking phenomenon. The properties of the cloud were taken from previous investigations and were not ‘fine tuned’ for this work. Had the column density been significantly smaller than assumed, the lines would have been optically thin (and hence undetectable in this study) and the cloud would also have been stable. Had the column density been significantly larger, the lines would have been far more optically thick and self-shielded, with the acceleration falling precipitously as a consequence. Such a cloud would fragment over scales corresponding to roughly optical depth unity in the driving lines. In fact, for these assumed properties, the cloud has precisely these properties. Could the currently visible, line-locked, small column density clouds be the result of radiative instabilities in a cloud which was originally considerably larger? Such a scenario might explain why the line-locking signature for the narrow absorbers is also present among the BALQSO sample. Alternatively, in a model in which BAL features are due to winds above the accretion disk, seen only for special viewing angles, the narrow absorption systems studied in this paper could result from the outwardly accelerated interstellar medium of the host galaxy, visible for a much larger range of viewing angle.

7 CONCLUSIONS

Investigation of the statistics of strong, narrow C IV doublet absorbers present in outflows seen in a large sample of luminous quasars ($-25.0 \lesssim M_i \lesssim -27.0$) demonstrates that line-locked C IV absorber doublets are an almost ubiquitous feature of outflows. From the samples of $\approx 31\,000$ non-BAL and ≈ 2600 BAL quasars it is found that:

- Approximately two thirds of quasars with multiple C IV absorption systems in outflows extending to $\sim 12\,000\text{ km s}^{-1}$ possess line-locked C IV absorbers, visible as C IV absorber triplets.
- The line-locked absorbers are present in both the non-BALQSO and BALQSO samples with comparable frequencies, suggesting a common origin for the acceleration of the clouds traced by the narrow C IV absorbers in non-BAL and BAL quasars.
- Line-locked C IV systems are present in outflows with velocities reaching at least $20\,000\text{ km s}^{-1}$.
- There are no detectable differences in the absorber properties and the dust content of single C IV doublets and line-locked C IV doublets.
- The gas associated with both single and line-locked C IV narrow absorption systems produces strong absorption due to species with a wide range of ionization potential (15 eV (Mg II) to 98 (N V) and even 138 eV (O VI)).
- Both single and line-locked C IV absorber systems show strong systematic trends in their ionization as a function of outflow velocity β . The ratio of the EW of N V₁₂₃₉ to C IV₁₅₄₈ decreases with increasing β , while that of Mg II₂₇₉₆ to C IV₁₅₄₈ increases.
- The current sample of absorbers from the SDSS DR7 quasars does not provide useful constraints on the prevalence of

line-locks with velocity separations $\gtrsim 1000\text{ km s}^{-1}$, including those due to N V and O VI at 964 km s^{-1} and 1654 km s^{-1} respectively.

- Simulations employing CLOUDY demonstrate that a rich spectrum of line-locked signals at various velocities may be expected due to significant opacities from resonance lines of Li-like, He-like and H-like ions of O, C and N, along with contributions from He II and H I resonance lines.

- Computing the line optical-depth autocorrelation function (ACF) for the full AGN SED spectrum for parameters taken from published models provides a quantitative way to assess the importance of overlapping lines.

- Many strong contributors to the ACF are found, particular those from O VI, N V and C IV doublets but, in the general case, the C IV doublet lock is not the strongest.

- The strength of particular line-locks depends on the shape of the illuminating AGN SED, which provides the photons responsible for the acceleration at the wavelength of each absorber species. The C IV line-lock can be made to appear significantly stronger by adopting an AGN SED shape in the ultraviolet to near X-ray range that is consistent with current knowledge of the AGN SED.

- The CLOUDY simulations confirm that line driving is the dominant acceleration for clouds with a column of $N(\text{C IV}) \approx 10^{14}\text{ cm}^{-2}$ and $N(\text{H}) \approx 10^{19}\text{ cm}^{-2}$. The outward acceleration falls by a factor of two across our fiducial cloud, showing that the flow is Rayleigh-Taylor unstable. Such a flow will fragment over scales similar to that observed—the point where the acceleration has fallen by a moderate factor. Could the clouds we observe be the result of such fragmentation of clouds that were originally significantly larger?

The observational results presented open up a potentially important new constraint for i) understanding the origin of the accelerating mechanism for high-ionization outflows in quasars and ii) the physical conditions pertaining within the flow. Observationally, improved constraints on the frequency of line-locks due to other species will be possible through the analysis of the forthcoming release (DR11) of the SDSS III quasar catalogue. Modelling outflows is a challenging, many-parameter, problem but the dependence of line-lock signatures from different species on the form of the AGN SED is a particularly promising direction for future work, on which we intend to embark. The improved statistics from the SDSS III quasar sample will also provide detailed determinations of the outflow cloud properties over an extended range in β .

ACKNOWLEDGEMENTS

We thank the anonymous referee for a constructive and thoughtful report and Fred Hamann for comments and discussions. Bob Carswell’s input, over an extended period, is much appreciated. PCH acknowledges support from the STFC-funded Galaxy Formation and Evolution programme at the Institute of Astronomy. JTA acknowledges the award of an STFC Ph.D. studentship and an ARC Super Science Fellowship. GJF acknowledges support by NSF (1108928, 1109061, and 1412155), NASA (10-ATP10-0053, 10-ADAP10-0073, NNX12AH73G, and ATP13-0153), and STScI (HST-AR-12125.01, HST-AR-13245, GO-12560, HST-GO-12309, and GO-13310.002-A), and is grateful to the Leverhulme Trust for support via the award of a Visiting Professorship at Queen’s University Belfast (VP1-2012-025).

Funding for the SDSS and SDSS-II has been provided by the Alfred P. Sloan Foundation, the Participating Institutions, the National Science Foundation, the U.S. Department of Energy,

the National Aeronautics and Space Administration, the Japanese Monbukagakusho, the Max Planck Society, and the Higher Education Funding Council for England. The SDSS Web Site is <http://www.sdss.org/>.

The SDSS is managed by the Astrophysical Research Consortium for the Participating Institutions. The Participating Institutions are the American Museum of Natural History, Astrophysical Institute Potsdam, University of Basel, University of Cambridge, Case Western Reserve University, University of Chicago, Drexel University, Fermilab, the Institute for Advanced Study, the Japan Participation Group, Johns Hopkins University, the Joint Institute for Nuclear Astrophysics, the Kavli Institute for Particle Astrophysics and Cosmology, the Korean Scientist Group, the Chinese Academy of Sciences (LAMOST), Los Alamos National Laboratory, the Max-Planck-Institute for Astronomy (MPIA), the Max-Planck-Institute for Astrophysics (MPA), New Mexico State University, Ohio State University, University of Pittsburgh, University of Portsmouth, Princeton University, the United States Naval Observatory, and the University of Washington.

REFERENCES

- Adams M. T., Coleman G. D., Stockman H. S., Strittmatter P. A., Williams R. E., 1978, *ApJ*, 223, 758
- Allen J. T., Hewett P. C., Maddox N., Richards G. T., Belokurov V., 2011, *MNRAS*, 410, 860
- Arav N., 1996, *ApJ*, 465, 617
- Arav N., Li Z.-Y., 1994, *ApJ*, 427, 700
- Arav N., Li Z.-Y., Begelman M. C., 1994, *ApJ*, 432, 62
- Arav N., Korista K. T., Barlow T. A., Begelman, 1995, *Nature*, 376, 576
- Baldwin J. A., 1977, *ApJ*, 214, 679
- Baskin A., Laor A., Hamann F., 2013, *MNRAS*, 432, 1525
- Benn C. R., Carballo R., Holt J., Vigotti M., González-Serrano J. I., Mack K.-H., Perley R. A., 2005, *MNRAS*, 360, 1455
- Blandford R. D., Payne D. G., 1982, *MNRAS*, 199, 883
- Borra E. F., et al., 1996, *AJ*, 111, 1456
- Bottorff M., Korista K. T., Shlosman I., Blandford R. D., 1997, *ApJ*, 479, 200
- Braun E., Milgrom M., 1989, *ApJ*, 342, 100
- Burbidge E. M., Burbidge G. R., 1975, *ApJ*, 202, 287
- Cardelli J. A., Clayton G. C., Mathis J. S., 1989, *ApJ*, 345, 245
- Castor J. I., 1974, *MNRAS*, 169, 279
- Castor J. I., Abbott D. C., Klein R. I., 1975, *ApJ*, 195, 157
- Chelouche D., Netzer H., 2001, *MNRAS*, 326, 916
- Chelouche D., Netzer H., 2003, *MNRAS*, 344, 233
- Coleman G., Carswell R. F., Williams R. E., Baldwin J., Robinson L. B., Wampler E. J., Strittmatter P. A., 1976, *ApJ*, 207, 1
- Cooksey K. L., Kao M. M., Simcoe R. A., O'Meara J. M., Prochaska J. X., 2013, *ApJ*, 763, 37
- Cottis C. E., Goad M. R., Knigge C., Scaringi S., 2010, *MNRAS*, 406, 2094
- Emmering R. T., Blandford R. D., Shlosman I., 1992, *ApJ*, 385, 460
- Fechner C., Baade R., Reimers D., 2004, *A&A*, 418, 857
- Ferland G. J., et al., 2013, *RMxAA*, 49, 137
- Foltz C. B., Weymann R. J., Morris S. L., Turnshek D. A., 1987, *ApJ*, 317, 450
- Ganguly R., Brotherton M. S., 2008, *ApJ*, 672, 102
- Ganguly R., Masiero J., Charlton J. C., Sembach K. R., 2003, *ApJ*, 598, 922
- Hamann F., Ferland G., 1999, *ARA&A*, 37, 487
- Hamann F., Kanekar N., Prochaska J. X., Murphy M. T., Ellison S., Malec A. L., Milutinovic N., Ubachs W., 2011, *MNRAS*, 410, 1957
- Hewett P. C., Foltz C. B., 2003, *AJ*, 125, 1784
- Hewett P. C., Irwin M. J., Bunclark P., Bridgeland M. T., Kibblewhite E. J., He X. T., Smith M. G., 1985, *MNRAS*, 213, 971
- Hewett P. C., Wild V., 2010, *MNRAS*, 405, 2302
- Jin, C. and Ward, M. and Done, C., 2012, *MNRAS*, 425, 907
- Konigl A., Kartje J. F., 1994, *ApJ*, 434, 446
- Korista K. T., Voit G. M., Morris S. L., Weymann R. J., 1993, *ApJS*, 88, 357
- Kruczek N. E., et al., 2011, *AJ*, 142, 130
- Kurosawa R., Proga D., 2009, *ApJ*, 693, 1929
- Lee D. D., Seung H. S., 1999, *Nat*, 401, 788
- Lee D. D., Seung H. S., 2000, *Advanced Neural Inf. Processing Syst.*, 13, 556
- Mathews, W., G., 1982, *ApJ*, 252, 39
- Milne E. A., 1926, *MNRAS*, 86, 459
- Murray N., Chiang J., Grossman S. A., Voit G. M., 1995, *ApJ*, 451, 498
- Nestor D., Hamann F., Rodríguez Hidalgo P., 2008, *MNRAS*, 386, 2055
- Ostriker J. P., Choi E., Ciotti L., Novak G. S., Proga D., 2010, *ApJ*, 722, 642
- Owocki S. P., Castor J. I., Rybicki G. B., 1988, *ApJ*, 335, 914
- Pâris I., et al., 2014, *A&A*, 563, A54
- Proga D., Jiang Y.-F., Davis S. W., Stone J. M., Smith D., 2014, *ApJ*, 780, 51
- Proga D., Ostriker J. P., Kurosawa R., 2008, *ApJ*, 676, 101
- Proga D., 2007, *ASPC*, 373, 267
- Proga D., Stone J. M., Kallman T. R., 2000, *ApJ*, 543, 686
- Savage B. D., Jenkins E. B., 1972, *ApJ*, 172, 491
- Savage B. D., Sembach K. R., 1991, *ApJ*, 379, 245
- Scargle J. D., 1973, *ApJ*, 179, 705
- Schlegel D. J., Finkbeiner D. P., Davis M., 1998, *ApJ*, 500, 525
- Schneider D. P., et al., 2007, *AJ*, 134, 102
- Schneider D. P., et al., 2010, *AJ*, 139, 2360
- Shen Y., et al., 2011, *ApJS*, 194, 45
- Shlosman I., Vitello P. A., Shaviv G., 1985, *ApJ*, 294, 96
- Simon L. E., Hamann F., 2010, *MNRAS*, 409, 269
- Srianand R., 2000, *ApJ*, 528, 617
- Tripp T. M., Lu L., Savage B. D., 1997, *ApJS*, 112, 1
- Urry C. M., Padovani P., 1995, *PASP*, 107, 803
- Vanden Berk D. E., et al., 2001, *AJ*, 122, 549
- Weymann R. J., Morris S. L., Foltz C. B., Hewett P. C., 1991, *ApJ*, 373, 23
- Wild V., Hewett P. C., 2005, *MNRAS*, 358, 1083
- Wild V., et al., 2008, *MNRAS*, 388, 227
- Williams R. E., Strittmatter P. A., Carswell R. F., Craine E. R., 1975, *ApJ*, 202, 296
- Vilkoviskij E. Y., Irwin M. J., 2001, *MNRAS*, 321, 4
- Vilkoviskij E. Y., Lovelace R. V. E., Pavlova L. A., Romanova M. M., Yefimov S. N., 2006, *Ap&SS*, 306, 129